ELSEVIER

Contents lists available at ScienceDirect

Reliability Engineering and System Safety

journal homepage: www.elsevier.com/locate/ress



Seismic fragility estimation of electrical substations accounting for component damage and short circuit faults

Nicolás Ahumada ^{a,*}, Juan Pablo Muñoz Gálvez ^{b,*}, Alan Poulos ^{b,1}, Félix Rojas ^c, Juan Carlos de la Llera ^{a,*}

- a Department of Structural and Geotechnical Engineering, Pontificia Universidad Católica de Chile, Santiago, Chile
- ^b Research Center for Integrated Disaster Risk Management (CIGIDEN), ANID/FONDAP/1523A0009, Santiago, Chile
- ^c Department of Electrical Engineering, Pontificia Universidad Católica de Chile, Santiago, Chile

ARTICLE INFO

Keywords: Electrical substation equipment Lifeline systems Probabilistic models Seismic fragility Substation system Reliability Resilience

ABSTRACT

Modern society relies heavily on electricity, which is transmitted from generating stations to final consumers through an electrical power grid. Electrical substations are key components of these grids. Previous earthquakes have heavily damaged some of these substations, affecting their functionality and leading to service interruptions. Functionality losses are usually modeled using fragility functions, which in general terms relate a seismic intensity measure with the probability of failure. Most previous studies use generic substation fragility functions that are not specific to the modeled substations. Indeed, power substations are composed of several internal components laid out in a wide range of different configurations, which cannot be accurately represented by these generic models. This study proposes a method to construct fragility functions based on the internal configuration of substation components and accounts for faults to individual lines within the substation and short circuit faults that render all the substation nonfunctional. The proposed method was applied to Chilean substations, resulting in fragility functions that vary significantly depending on their voltage level and their internal configuration. On average, the resulting fragility functions are fairly similar to the generic functions provided by HAZUS. However, fragility functions of individual substation archetypes can differ significantly between each other and with those of HAZUS. Thus, using fragility functions that consider a more realistic internal configuration of electrical components instead of generic functions can improve estimations of seismic performance, risk, and resilience of electric power grids, and hence help in providing better tools to prepare and mitigate earthquake effects.

1. Introduction

The Electrical Power Grid (EPG) infrastructure occupies an essential role in modern societies because human settlements depend on electric energy for a myriad of different uses, including domestic and industrial activities, public services such as street illumination and traffic lights, and hospital operations. Several critical lifelines depend on EPG, including water treatment and distribution, transportation, telecommunications, and healthcare, among others. Thus, a failure in the grid may have a severe impact on the overall functioning of society, produce a substantial economic loss, and potentially affect millions of people (e. g., [1–3]). A key type of EPG component is the Electric Power Substation (EPS) because it works as a node between generation plants,

transmission lines, and the final user's voltage level. Past earthquakes have shown that EPSs are vulnerable to damage and malfunctioning under seismic loads, which may cause important interruptions to power flow (e.g., [4,5]). Moreover, past earthquakes have also shown that EPSs tend to be more vulnerable than other types of transmission components of the EPG, such as transmission towers ([6]). Thus, characterizing the performance of EPSs when subjected to earthquake loads is a key step in evaluating the seismic risk and resilience of the EPG, which in turn can be used to propose mitigation strategies that improve seismic resilience of the overall society.

Typical seismic risk and resilience analyses of EPGs consider every component (e.g., generators and substations) to be in different possible states of damage, which are estimated using fragility functions (e.g.,

^{*} Corresponding authors.

E-mail addresses: nyahumada@uc.cl (N. Ahumada), jpmunoz4@uc.cl (J.P. Muñoz Gálvez), jcllera@uc.cl (J. Carlos de la Llera).

 $^{^{\}rm 1}$ Now at U.S. Geological Survey, Moffett Field, CA 94035.

[7–13]). More recently, significant research has focused on developing advanced probabilistic frameworks to assess and improve the seismic resilience of substations, considering aspects such as multi-stage uncertainties, equipment-to-equipment failure correlations, and the identification of critical components [14-18]. The cornerstone of these modern analyses is the estimation of damage states using fragility functions. In summary, fragility functions are cumulative distribution functions that describe the probability of reaching or exceeding different states of damage given an Intensity Measure (IM) of ground shaking (e. g., peak ground acceleration). While functions derived directly from empirical damage data are ideal, their development is often hindered by the scarcity of detailed, component-level post-earthquake information. This is particularly true for complex systems like electrical substations, where post-event data is rarely sufficient for robust statistical calibration. Consequently, the development of analytical fragility models, which are grounded in the physical and mechanical properties of the components and their system configuration, becomes a critical necessity for performing reliable seismic risk and resilience assessments. This study addresses that need by proposing such a methodology.

The selection or construction of adequate fragility functions is of utmost importance because they greatly affect the outputs of a risk and resilience analysis. In the case of FEMA-HAZUS [19], five states of damage are considered for the seismic fragility of an EPS: operational, slight, moderate, extensive, and complete. Some researchers have focused on obtaining fragility functions for EPS starting with their component fragilities [20-23], and including uncertain factors [24], while others have studied the failure of specific EPS components, such as high voltage disconnect switches [25,26]; porcelain high voltage insulators [27]; high voltage power transformers [28]; power circuit breakers [29]; and the relative vulnerability of different components [30]. Also, initiatives like SYNER-G and HAZUS employ substation models that represent complex electrical systems with multiple interconnected components [19,31]. Although prior studies have shown that using multiple intensity measures as input or for classifying ground motions reduces the uncertainty of fragility functions (e.g., [32,33]), this study uses only PGA to maintain a direct basis for comparison with the HAZUS framework.

Fragility functions from HAZUS are widely used and were obtained through numerical modeling and a Boolean approach. The typical fragility functions used by HAZUS were derived by the probabilistic combination of component damage and their functional relations, and then by computing the percentage of broken components within the substation. The three main components examined this way were the circuit breakers, the disconnect switches, and the power transformers. Each damage state has an associated threshold value for the percentage of broken components, namely, 5 %, 40 %, 70 %, and 100 % for slight, moderate, severe, and total damage, respectively.

While the previous approach may be practical, it fails to acknowledge the operational consequences of the failure of the different EPS components, given their position in parallel and in series with respect to others. For instance, if an EPS has only one input line at the very beginning of the circuit and it fails, power will not flow through the substation and the damage should be complete, regardless of the percentage of broken components. Furthermore, it also does not consider the inner typologies or arrangements of different substations, thus two EPS with very different internal redundancies are considered to behave the same, which is not the case. For example, Liu et al. modeled all the substations in their study as single busbar [23], whereas Li, Wang and Shang modeled them as double busbar [22], but neither of them made any adjustment for any other typologies. Also, previous studies have not considered short circuit failure, which requires an adequate clearance model. Short circuit failures, unlike overloads or line disconnections, involve direct contact between points of different electrical potential, leading to excessive current flow and potentially severe damage to critical components. If not properly managed, these failures can disable entire substation and cause cascading blackouts

interconnected systems. Hence, it is necessary to develop more precise fragility functions for EPS to account for these factors.

This study develops a method to derive fragility functions of EPSs considering their inner configuration of components. The fragility of individual EPS components is constructed by multiple stripe analysis [34] using dynamic simulations with components designed following current seismic provisions (e.g., [35–38]). Monte Carlo simulations are then used to sample the damage states of EPS components, which are included in a fault tree analysis to estimate the percentage of current that flows through the EPS and the presence (or not) of a short circuit failure. The simulation results are assembled to construct fragility functions of the EPS. This proposed method is applied to develop fragility functions of most EPS in Chile, which are then classified in a set of clusters based on their similarity, representing different substation archetypes. The proposed method can be used to construct fragility functions for the study of seismic risk and resilience of electric power grids located in seismically active regions (e.g., [9,39]).

2. Substation layouts

Electric power systems are composed of three sectors whose activities make the provision of electric energy possible. The generation sector oversees the production of electric energy through different renewable and non-renewable sources such as hydroelectric, solar, wind, and thermoelectric. The transmission sector efficiently transfers, at high voltage levels, the produced energy to all nodes of the system, through transmission lines. The distribution sector carries electricity from the transmission substation to final consumers, progressively reducing the voltage levels from high-voltage transmission lines to low-voltage distribution lines, which is performed at the electrical substations. These substations contain several electrical components in different layouts, which will be described in this section.

2.1. Substation components

To obtain reliable fragility functions of electric power substations, the seismic behavior of their electrical components is needed. This study considers five critical components of substations, which are shown in Fig. 1: (i) the power transformer, which plays a pivotal role in changing voltage without altering frequency and are used for a wide range of voltage transformation requirements, allowing power distribution and efficient long-distance electricity transmission; (ii) the circuit breaker, which serves as a mechanical device to connect or disconnect various elements within the system, handling abnormal conditions like short circuits and maintenance tasks while adhering to specified admissible short circuit current durations; (iii) disconnect switches also play an important role because they are used in circuit division and system component isolation for maintenance or short-circuit fault clearance, ensuring mechanical integrity during peak short-circuit conditions; (iv) potential transformers are also critical and function as measurement points to faithfully replicate high-voltage circuit effects in the lowvoltage circuit, making them essential for waveform quality and harmonic analysis; and finally, (v) current transformers facilitate current measurements and mitigate voltage peaks in different system lines, contributing to precise monitoring and control.

2.2. Substation classifications

Substations can be categorized according to their function (switching, pure transformation, or transformation-switching), the voltage level transformation (step-up or step-down), the placement of its components (outdoor or indoor installation), the insulation of their components (insulated in air, gas, or a hybrid manner), or according to the voltage level, as categorized in this article following the indications of the National Electric Coordinator (NEC) [40] (Extra High Voltage—EV, High Voltage—HV, and Medium Voltage—MV).



Fig. 1. Electric power substation components: (a) power transformer, (b) disconnect switch, (c) circuit breaker, (d) current transformer, and (e) potential transformer.

Substations are also classified according to the layout of their internal components, which can be represented by a single-line diagram. Single-line diagrams are orthogonal schemes that graphically represent an electrical installation through simple graphical lines and symbols, without necessarily following the geospatial location of the electrical equipment. They provide detailed information on the electrical connections between components, illustrating their interconnected destinations and relationships. The substation layouts studied in this work are presented with single-line diagrams in Fig. 2, and correspond to: (a) the single busbar configuration, characterized by a single collector busbar connected to circuits through circuit breakers, known for its cost-effectiveness, simplicity, protection ease, and space efficiency; (b) the single and transfer busbar configuration, designed to enhance reliability by adding an auxiliary or transfer busbar with disconnect switches for circuit connection and a transfer circuit breaker to connect both busbars,

with only the main busbar energized under normal conditions; (c) the double busbar configuration, which introduces a second energized busbar and a coupling circuit breaker to provide flexibility and facilitate circuit separation, thereby enhancing system division; and (d) the tap off configuration, designed for small substations interconnecting multiple circuits to diversify power supply sources and improve the overall reliability of the grid. These four substation layouts were selected for this study as they represent the vast majority (over 95 %) of the high-voltage substations in the Chilean electrical power grid. Therefore, they are the most relevant configurations for a seismic risk and resilience analysis of this specific network. The symbology defined by the IEE315 standard [41] is used to indicate each component.

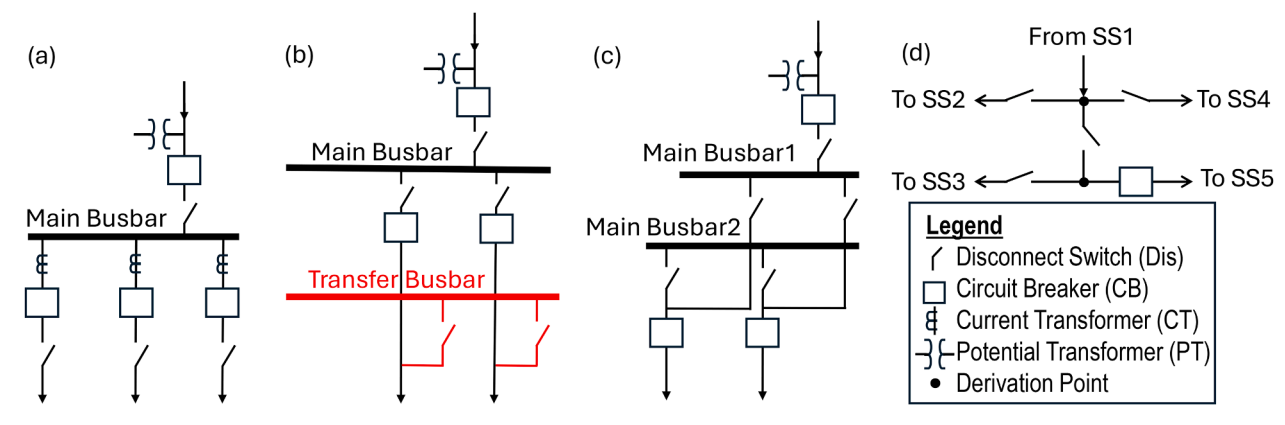


Fig. 2. Single-line diagrams: (a) single busbar; (b) single and transfer busbar; (c) double busbar; and (d) tap off substation (SS) layouts.

2.3. Chilean substations

This article uses the substations of the Chilean National Electric System (SEN), which covers most of the national territory and serves 98.5 % of the Chilean population [42]. An official open repository with SEN data was accessed [43] to obtain information on Chilean substations, including single-line diagrams. The existing substation database was curated and completed based on the single-line diagrams to classify each substation that forms part of the SEN by its voltage level, layout, and the number of its different types of lines, namely, line-in, transformation lines, and line-out. The map shown in Fig. 3 shows the distribution of these substations.

3. Component fragilities

The seismic response of the different components that make up a substation was analyzed by means of a series of nonlinear time-history analyses. These numerical models were used to simulate the dynamic responses of the components to three-dimensional earthquake ground motions. Component failure was then estimated based on the seismic response of the porcelain elements of the insulators, which previous studies have shown to control failure due to their brittleness and lack of ductility [28,44,45].

3.1. Component models

Substation components were modeled and analyzed with the SAP2000 software [46]. As shown in Fig. 4, each component, except for the power transformer, consisted of a porcelain element or a set of porcelain elements supported by a steel structure. The current and potential transformers consist of a single porcelain element, while the disconnect switches and circuit breakers consist of six porcelain elements. Porcelain elements were represented by frame elements with a Young modulus of 70 GPa, a Poisson coefficient of 0.17, and a mass density of 2,500 kg/cm³. The geometry of their circular cross-sections depended on their voltage levels, varying from 25 to 35 cm for medium voltage, 130 to 200 cm for high voltage, and 220 to 350 cm for extra high voltage. The steel support structures were also modeled using frame elements that represented L and C cross-sections, specifically, L80 \times 80 \times 6 mm and C100 \times 50 \times 5 mm for the beams and columns, and L40 \times 40 \times 4 mm and C100 \times 75 \times 5 mm for the diagonal members of the trusses. A minimum height of 230 cm was considered for the support structures, and the steel was characterized by a Young modulus of 200 GPa, a Poisson coefficient of 0.3, and a mass density of 7,865 kg/cm³.

The numerical models defined the boundary conditions at the base of the steel support structures as fully fixed, representing a rigid connection to the foundation. To accurately reflect typical construction practices, the connections for the diagonal bracing members were modeled as pinned, releasing their rotational degrees of freedom. The assumption of a fixed base is considered conservative for assessing the fragility of the porcelain insulators, as it maximizes the transfer of ground motion energy into the superstructure, thereby maximizing the bending and shear

demands on these critical, brittle components. It is also noted that the dynamic interaction effects from interconnected flexible conductors (i. e., suspended connections) were not explicitly modeled, as each piece of equipment was analyzed individually. Instead, their influence is represented by equivalent static forces applied to the components as stipulated by the governing design standards.

The components were designed following the standards that govern the seismic design of electrical installations in Chile [29,30]. These standards require the supporting structure to have a fundamental vibration frequency greater than or equal to 30 Hz and that all elements with fragile failure modes (e.g., porcelain elements) must have a minimum safety factor of 2, considering shear and bending. They also consider static loads acting alongside the earthquake loads (E) at different points of the components, namely dead loads (D), connection loads (T), short-circuit loads (SC), and operating loads (OP). These loads are usually defined by the supplier and must be combined in the most unfavorable direction of each type of load, according to Eq. (1).

Load Combination =
$$D + E + OP + T + 0.6 \cdot SC$$
 (1)

Short-circuit loads are modeled as a static force that represents the effect of the short circuit on the component, calculated according to Eq. (2):

$$SC = \frac{0.0204(2.5 \cdot I_c)^2 \cdot L}{d}$$
 (2)

where L is the length (in meters) through which the short-circuit current flows (normally 1 m in addition to the length of the insulator), d corresponds to the phase separation (in meters), I_c is the short-circuit's root mean square current (in kA), and SC is given in daN. Solicitations due to connection loads (T) have a value of 100 daN, and in the same way as short-circuit forces, they are applied at the terminal or upper end of the insulator. Finally, operating loads (OP), provided by the equipment supplier, reflect the forces and movements associated with the normal operation of the equipment, such as the opening or closing of a disconnect switch. Note that the load combination procedure of Eq. (1) does not explicitly model the dynamic interaction effects of interconnected flexible conductors (i.e., suspended connections), as each piece of equipment was analyzed individually.

3.2. Ground motion selection

Time-history analyses were carried out for each EPS component to derive their fragility functions using Multiple Stripe Analysis (MSA) [34]. With this in mind, a consistent set of ground motion records was selected from a Chilean strong-motion database [47] to match 20 Conditional Spectra (CS) with PGA values between 0.2 g and 2.4 g, equivalent to return periods between 50 and 10,000 years. For each CS, 30 bidirectional horizontal ground motion records were selected using the algorithm proposed by Baker and Lee [48], as shown in Fig. 5. The CS were constructed using the method proposed by Lin et al. (2013) and the seismic hazard of a substation located in the coastal city of Reñaca with an average shear wave velocity in the top 30 m of soil ($V_{\rm s30}$) of 425 m/s

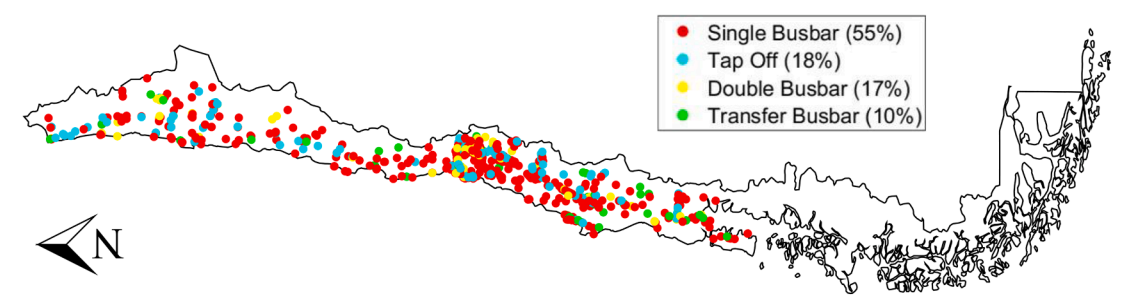


Fig. 3. Geographical distribution of SEN substations within Chilean territory according to their layout.

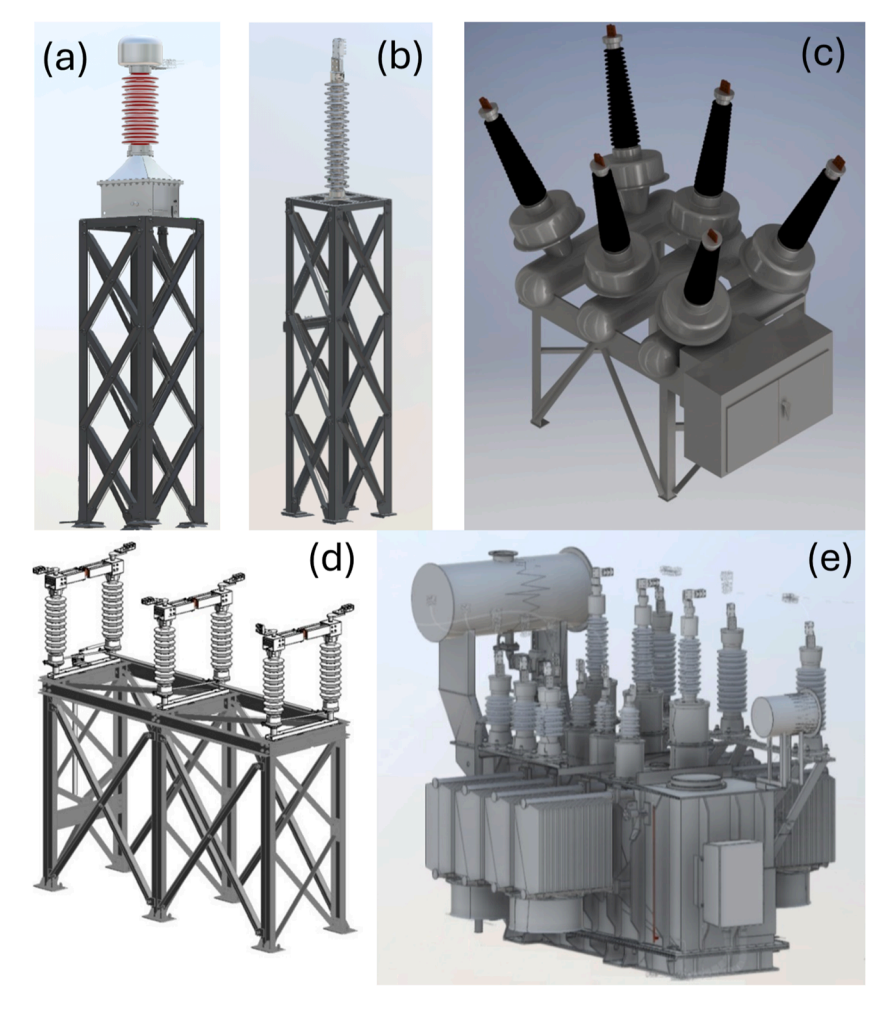


Fig. 4. Geometric models of (a) potential transformer, (b) current transformer (c) circuit breaker, (d) disconnect switch, and (e) power transformer.

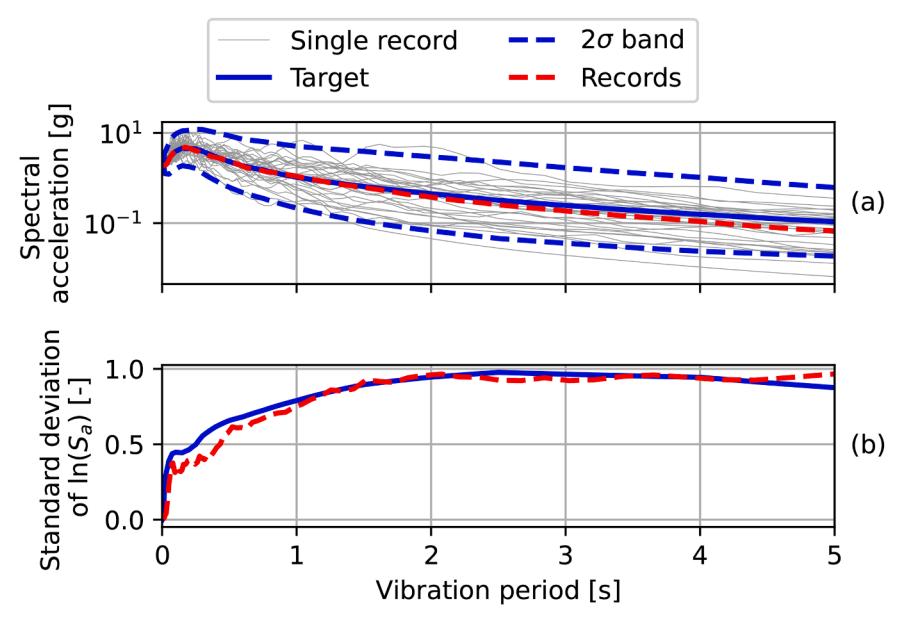


Fig. 5. Selection of 30 ground motion records to match the conditional spectrum at a PGA value of 1.87 g. (a) Response spectra of the selected ground motions with their geometric mean matching the target conditional mean spectrum (CMS). (b) Standard deviation of the logarithms of the response spectra matching the target conditional standard deviation.

(soil type C in the Chilean seismic code [49]). The fragility functions that resulted from these ground motions were used for all substations. Thus, future work may study the effect of using sites with different soil types or locations relative to the subduction interface on the fragility functions. The seismic hazard was estimated by combining five ground motion models, namely, [50–54], with equal weights; the Strasser et al. (2010) [55] model for scaling seismic source dimensions; and the recurrence model of Poulos et al. (2019) [56] of Chilean subduction sources. A maximum scaling factor of 10 was used for both horizontal components to increase the pool of candidate records for very large PGA values. The vertical component was scaled so its peak acceleration corresponds to 60 % of that of the horizontal component, following the recommendation of the Chilean standard [36].

3.3. Assessment of electrical component fragilities

The seismic fragility of a component refers to the conditional probability that it exceeds a certain limit state under the action of different ground motion intensity levels. For this case, the fragility function was characterized by the cumulative distribution function of a lognormal probability distribution [57] with a median value θ and logarithmic standard deviation β , as shown in Eq. (3):

$$P(LS|IM = im) = \Phi\left(\frac{\ln(im/\theta)}{\beta}\right)$$
(3)

where P(LS|IM=im) indicates the conditional probability that a ground motion with intensity IM=im (in this case, peak ground acceleration, PGA) will cause a component to exceed a predefined limit state LS, and $\Phi(\cdot)$ represents the cumulative distribution function of a standard normal probability distribution.

For each component type, a model was built as explained in Section 3.1 and analyzed with the seismic records presented in Section 3.2. A single limit state is considered for each one of its porcelain insulators, corresponding to the state at which they fail to perform their function. The component limit state is defined by a safety factor, calculated as the ratio of structural capacity to seismic demand for both shear and bending. Capacity (V_c , M_c) is the ultimate shear and moment resistance of the critical porcelain insulators, derived from material strength and cross-sectional properties. Demand (V_d , M_d) is the peak internal force obtained from the nonlinear time-history analyses, evaluated at the base of the porcelain insulators where bending and shear stresses are highest. The failure criterion is adopted directly from the governing Chilean

standard [29], which explicitly requires that fragile elements maintain a minimum safety factor of 2.0 against either shear or bending failure under the combined design loads. Therefore, a component is considered to have failed if its Safety Factor for shear (V_c/V_d) or bending (M_c/M_d) drops below this required threshold. Consequently, the single Safety Factor value shown in Fig. 6a represents the minimum of these two values for each simulation. It is important to note that for all simulations, the steel support structures remained well within their elastic capacity, confirming that failure was consistently governed by the brittle behavior of the porcelain insulators. Example MSA results are presented in Fig. 6a for the case of a current transformer in extra high voltage, showing the safety factors at the different stripes (i.e., levels of PGA).

Once the MSA results were obtained, the fragility functions were derived by first computing the fraction of ground motions at each stripe that caused safety factors lower than 2, and then fitting a lognormal probability distribution using maximum likelihood estimation [50]. The fragility function fitted to the example MSA results is presented in Fig. 6b.

An important consideration for the obtained results is that Chilean standards require a damping ratio of $\xi=2\%$ for all components [36], which was considered in the analyses. However, tests of hollow-core composite insulators have shown that the average damping ratio ranges from 0.6 % to 1.1 % [58,59]. Hence, the fragility functions were also obtained for damping ratios of 0.5 % and 1 %, as presented in Fig. 7a for the example component, which shows that the brittle component becomes more fragile as damping decreases. The figure also compares the derived fragility functions to the function defined by HAZUS [19] for current transformers. The HAZUS fragility function suggests a lower probability of failure at comparable levels of PGA. This discrepancy underscores the necessity of developing tailored fragility models that more accurately capture the seismic vulnerabilities of substation components, particularly in regions with specific seismic design requirements.

In addition to the damping ratio, another critical aspect affecting the seismic design of electrical components is their nominal voltage and component types. Higher nominal voltage typically indicates greater fragility in components, as it often results in taller insulators and, consequently, greater mass. This increased mass not only raises the seismic forces that the component must withstand but also elevates the center of gravity, further impacting the component's stability and seismic performance, as can be seen in Fig. 7b. Thus, each type of electrical component has three different versions, one for each of the voltage levels specified by the NEC [40], namely, extra high voltage (EV,

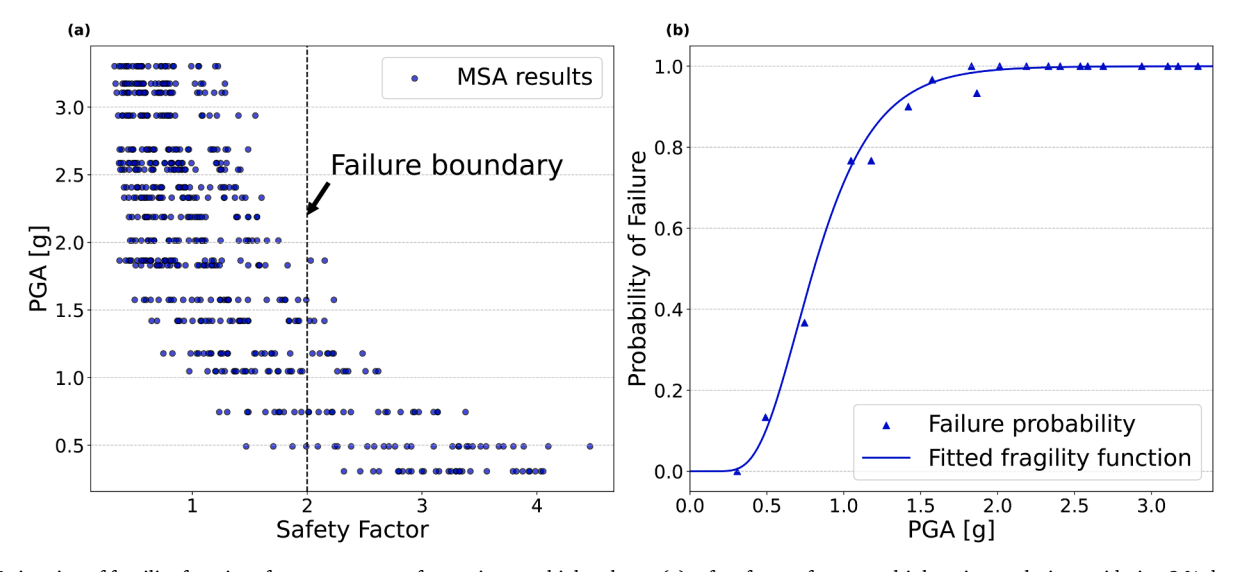


Fig. 6. Estimation of fragility functions for a current transformer in extra high voltage: (a) safety factors from a multiple stripe analysis considering 2 % damping; (b) fragility function fitted with maximum likelihood estimation for the 2 % damping case.

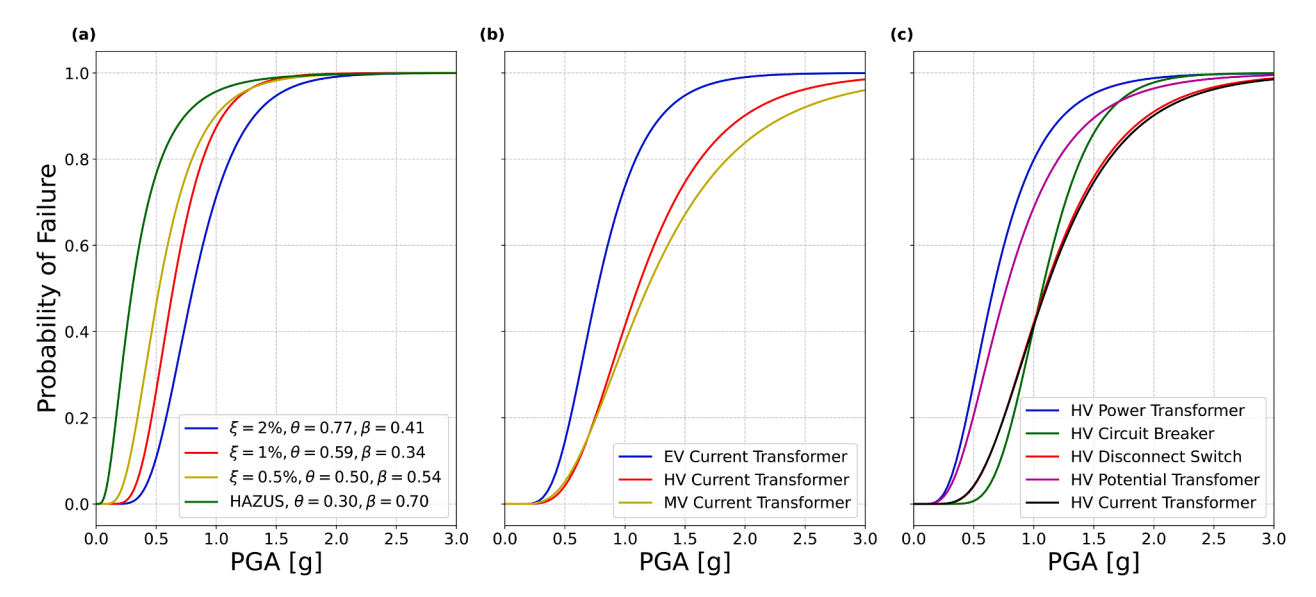


Fig. 7. Fragility functions of: (a) Current Transformer in extra-high voltage with different damping ratios compared to the HAZUS function; (b) Current transformers with different voltage levels; and (c) All substation component types in high voltage. Panels (b) and (c) assume 2 % damping ratio.

345 - 1,000 kV), high voltage (HV, 33 - 345 kV), and medium voltage (MV, 2.4 - 33 kV). HAZUS classifies voltages into high voltage (HV, 350 kV and above), medium voltage (MV, 150 kV to 350 kV), and low voltage (LV, 34.5 kV to 150 kV) [19]. While the Chilean EV and the HAZUS HV categories are comparable, a direct correspondence between the MV and LV categories of HAZUS and the HV and MV categories defined in the NEC is not straightforward due to differences in voltage ranges. A detailed comparison of the fragility functions based on these different classifications is presented in Section 5.

As stated before, each type of component was studied considering three values of damping ratio and three values of nominal voltage. The resulting parameters of the fragility function fitted for all analyzed components are presented in Table 1, which shows the median θ and the logarithmic standard deviation β of each case. As an example, Fig. 7c compares the fitted fragility functions of all components types at HV and 2 % damping.

3.4. Validation of the component fragility modeling approach

The failure criterion used in this study is based on a uniform safety factor of 2.0, a requirement mandated by the Chilean seismic design standard for fragile electrical components [29]. While this provides a consistent, code-based approach, it is acknowledged that this is a

Table 1Fragility function parameters for components of electrical substations.

Component	Voltage	$\xi=0.5\%$		$\xi=1\%$		$\xi=2\%$	
		θ	β	θ	β	θ	β
Circuit Breaker	EV	0.52	0.46	0.65	0.47	0.78	0.41
	HV	0.80	0.5	0.85	0.45	1.07	0.31
	MV	0.84	0.32	0.98	0.32	1.12	0.47
Current Transformer	EV	0.50	0.54	0.59	0.34	0.77	0.41
	HV	0.78	0.62	0.93	0.58	1.11	0.46
	MV	0.80	0.72	1.02	0.60	1.19	0.53
Potential Transformer	EV	0.52	0.54	0.64	0.42	0.73	0.44
	HV	0.52	0.63	0.68	0.55	0.77	0.53
	MV	1.35	0.26	1.42	0.25	1.48	0.23
Disconnect Switch	EV	0.64	0.56	0.68	0.52	0.79	0.49
	HV	0.85	0.37	0.88	0.39	1.09	0.45
	MV	1.90	0.37	2.12	0.34	2.20	0.32
Power Transformer	EV	0.37	0.47	0.38	0.42	0.4	0.42
	HV	0.61	0.37	0.63	0.38	0.66	0.49
	MV	0.65	0.42	0.71	0.44	0.75	0.40

simplification. To assess the reasonableness of this method, the resulting component fragility functions were compared against established models from the literature, such as those from HAZUS [19].

This comparison reveals a significant, yet insightful, discrepancy. For example, for the Extra-High Voltage Current Transformer with 2 % damping, our derived fragility function has a median (θ) of 0.77 g, whereas the corresponding HAZUS curve for anchored components has a median of 0.30 g. The other component types analyzed in this study were also found to be more resistant than their associated HAZUS counterparts. This general finding indicates that our model, which is based on components designed according to modern and stringent seismic provisions for a high-seismicity region like Chile, predicts a much higher seismic resistance than the generic HAZUS functions, which are intended for broader inventories that may include older equipment. This difference does not invalidate our approach; rather, it highlights the significant impact of applying region-specific, modern seismic design codes. Indeed, creating such tailored fragility functions is a valuable contribution, as many large-scale system resilience studies must rely on sourcing pre-existing fragility parameters directly from the literature to build their models [18].

4. Substation modeling

This section describes the method used to estimate the functionality of a substation after an earthquake as a function of the seismic damage to its electrical components, and how this information is processed to compute fragility functions. The method relies solely on the operational states of these components and their layout within the substation [60, 61]. The operational state of components is estimated with fragility functions, as explained in the previous section.

4.1. Operativity model

Consider a system, such as a substation, with a set C of n components. Each component is represented by a binary state variable x_i , with i=1, ..., n, which takes a value of 1 when the i-th component is operational, and 0 otherwise. The vector $\mathbf{x} = (x_1, ..., x_n)$ is called the state vector and indicates which components of the system are operational and which are out of service. Analogously, the operative state of the system only depends on the states of the components through a structure function $\phi(\mathbf{x})$ [60,61], which is based on its state vector \mathbf{x} , where system operativity is represented with a value of 1, and non-operativity with a value of 0.

The two most basic systems correspond to components in series and parallel arrangements. A series system is in operative state if and only if

each component is operative, therefore its structure function is $\phi(x) =$

$$\prod_{i=1}^{n} x_i = \min(x_1, ..., x_n).$$
 A parallel system is operative if and only if at least one component is operational, which translates to the structure

function $\phi(\mathbf{x})=1-\prod_{i=1}^n (1-x_i)=\max(x_1,...,x_n)$. For these simple cases, the system state may be described by a binary variable; however, more complex structure functions allow for a multi-state system. This study considers a system with $m\in\mathbb{N}$ possible operativity states and one non-operational state, making the complete state set:

$$\mathscr{S} := \left\{0, \frac{1}{m}, \frac{2}{m}, \dots, \frac{m-1}{m}, 1\right\} \tag{4}$$

where 1 represents perfect system operation, 0 its total system failure, and the other m-1 values correspond to intermediate states. These states are physically meaningful as they directly represent the fraction of a subsystem's parallel lines that remain functional. For a subsystem with m lines, a functionality state of i/m signifies that i out of m lines are operational. This approach models the degradation process not as a simple binary outcome (i.e., fully operational or completely failed), but as a gradual loss of capacity as individual lines are rendered non-operational. Thus, the functionality of a multi-state system with binary components may be defined by a structure function $\phi(x): \{0,1\}^n \to \mathcal{S}$.

Consider a multi-state structure function $\phi(x)$ and a system with n components and m possible states. Let us define a set of m associated binary systems, whose structure functions are given by:

$$\phi_i(x_1,...,x_n) = \begin{cases} 1, & \phi(x_1,...,x_n) \ge i/m \\ 0, & \phi(x_1,...,x_n) < i/m \end{cases}, \forall i = 1,...,m$$
 (5)

Therefore, a multi-state function may be determined as:

$$\Lambda = \phi(\mathbf{x}) = \frac{1}{m} \sum_{i=1}^{m} \phi_i(x_1, ..., x_n)$$
 (6)

A module (A,χ) is a subset of system components, A, organized in some substructure with structure function χ which can be treated as a component of the system. Thus, knowing whether χ is 1 or 0 (i.e., if the substructure is operational) is as informative as knowing the value of x_i for each component in A. A modular decomposition of the coherent system (C,ϕ) is a set of g disjoint and proper modules $\{(A_1,\chi_1),...,(A_g,\chi_g)\}$, where $C=\bigcup_{j=1}^g A_j$, and $A_j\cap A_f=\emptyset$, $\forall j\neq f$. The previous conditions imply that all components are considered in one module. Subset A_j corresponds to the j-th modular set of C, \mathbf{x}^{A_j} to the state vector of the components of A_j , and $\chi_j(\mathbf{x}^{A_j})$ to the state variable or structure function of the j-th module.

This article proposes a method to determine the functionality of a substation by considering three multi-state series systems: (i) I for the inlines, (ii) I for transformation lines, and (iii) I for out-lines. The set I for transformation lines, and (iii) I for out-lines. The set I for transformation lines, and (iii) I for out-lines. The set I functionality values of each of these subsystems. Crucially, each functionality value, I for operational lines within its respective subsystem. These values are obtained from the I for I for I for inclines, I transformation lines, and I sout-lines, respectively. The set of components of each system are I for I for I for I for inclines, and I for inclines, are spectively. Thus, each multi-state system is composed of binary components grouped in series and parallel. Each line is defined as a modular assembly, which has a binary structure function I by modeling each line as a modular assembly with binary structure functions, the proposed model accounts for the interdependency between the different stages of the substation.

Faults or malfunctions in the input lines can reduce or disrupt the flow of power to the transformation and output lines, ultimately affecting the overall functionality of the substation.

Suppose the in-line system has a total of r components organized in p lines. Let $\left\{ (A_1^I,\chi_1^I),..., \left(A_p^I,\chi_p^I\right) \right\}$ be the set of modules which forms a modular decomposition of the coherent multi-state system (C^I,ϕ^I) that offers a resolution for Λ^I . Subset A_k^I corresponds to the set of components of line $k \in I$ (i.e., a modular set) and ϕ_k^I is its structure function:

$$\phi_k^I = \chi_k^I \left(\mathbf{x}^{A_k^I} \right) \tag{7}$$

where $x^{A_k^I}$ is the state vector of the corresponding modular set A_k^I . Assuming that the in-lines are in parallel, and all have the same importance in the internal flow of the EPS, the state of the in-line system is:

$$\Lambda^I = \frac{1}{p} \sum_{k=1}^p \phi_k^I \tag{8}$$

A simple example is presented in Fig. 8 to better illustrate the previous concepts. The components of the system are $C^I = \{c_1, ..., c_r\}$, and each line may have a different number of them. In the example, the first line has four components, the second line has three components, and the p-th line has four components, and their corresponding modular sets are $A_1^I = \{c_1, c_2, c_3, c_4\}$, $A_2^I = \{c_5, c_6, c_7\}$, and $A_p^I = \{c_{r-3}, c_{r-2}, c_{r-1}, c_r\}$, respectively. Each line has its components in series, which results in the structure functions ϕ_k^I shown in Fig. 8, and Λ^I is computed using Eq. (7). An analogous procedure is used for the sets of transformation lines and out-lines, obtaining the functionality of Λ^T and Λ^O , respectively.

4.2. Failure modes

Fragility functions were developed based on two failure modes: line failures and short circuit clearance failures. These were modeled using independent fault trees. A detailed description of both failure modes is provided next.

4.2.1. Line failures

The first failure mode considers substation lines losing functionality due to seismic damage to substation components. Excessive acceleration induced by ground shaking may produce mechanical failure of electrical components, which may, in turn, cause some (or all) lines of the substation to stop transmitting electric power. Because different lines experience mechanical failure independently, this implies that the substation may experience intermediate states of damage. Hence, fault trees are used to evaluate the functionality of the substation as a multistate system, which considers both the seismic fragility of each component and the topology of the system.

The structure function for each line is derived following a clear set of rules based on its physical configuration. The general principle is that all components on a single line are considered to be in a series system. Physically, this means a line can only operate if every component along its path is functional. Mathematically, its structure function is the product of the state variables of its components ($\phi_i = \prod x_i$). The primary exception to this rule occurs in layouts with built-in redundancy, such as the double busbar (DB) configuration, whose structure function construction is explained later.

The functional state of the substation is then evaluated through fault trees that consider the operational status of its subsystems, i.e., in-lines, transformation lines, and out-lines, and depends on the internal layout, as explained later. Because the substation is a multi-state system, its functionality is determined by the combination in series of the proportion of operating lines of each subsystem separately, representing a flow of electricity circulating through the substation, as shown in Eq. (9):

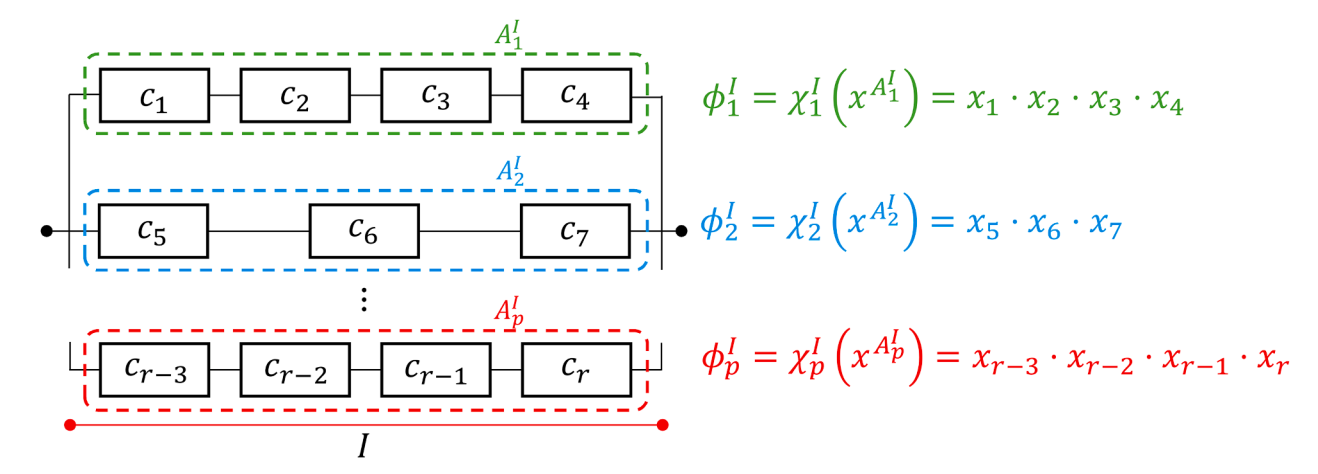


Fig. 8. Example of the modular sets of the in-lines of a substation.

$$\Lambda_{l} = \prod_{\omega \in \{l,T,O\}} \Lambda_{l}^{\omega} = \prod_{\omega \in \{l,T,O\}} \left(\frac{1}{|\omega|} \sum_{i=1}^{|\omega|} \phi_{i,l}^{\omega} \right)$$

$$\tag{9}$$

where $\phi_{i,l}^{\omega}$ corresponds to the state function of the i th line of type ω , with subscript l indicating that it is associated with line failures. Note that the vertical bars indicate the cardinality of a set. Current and potential transformers are not essential for the substation's internal electricity flow, as their role is primarily metering, allowing the substation to operate without them. This condition precludes their consideration in this particular failure mode.

As explained previously, the double busbar (DB) configuration, illustrated in Fig. 9, requires a different structure function because it contains transferred lines that are connected to both busbars using disconnects switches. These disconnect switches function as parallel components that are connected in series with other components of the transferred line. The transferred lines could be for any type of line,

provided they are connected to both busbars.

Given that both busbars are continuously energized, a failure scenario arises when both disconnect switches associated with a transferred line fail to operate. To model this scenario, a subset $\mathscr{L}^\omega \subset \omega \in \{I, T, O\}$ is introduced into the line failure analysis in this layout, which represents the transferred lines that are connected to both busbars. For these lines, the state function is computed assuming that the two disconnect switches (with state variables x_1 and x_2) are in parallel and that this system is in series with the rest of the components of the line, as shown in Eq. (10):

$$\phi_{i,l}^{\omega} = \begin{cases} (1 - (1 - x_1)(1 - x_2)) \prod_{i=3}^{n} x_i \ \forall i \in \mathscr{L}^{\omega} \\ \prod_{i=1}^{n} x_i \ \forall i \notin \mathscr{L}^{\omega} \end{cases}$$

$$(10)$$

where $x_3, ..., x_n$ represent the state variables of the rest of the compo-

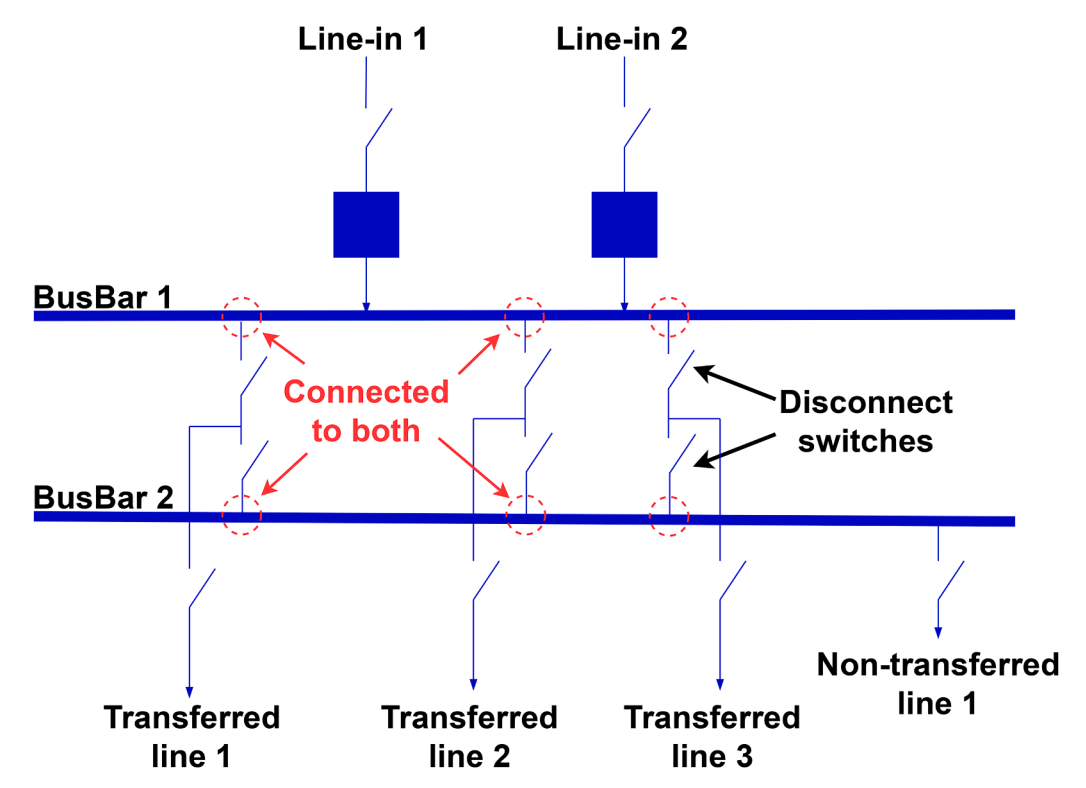


Fig. 9. Example of a double busbar configuration and its transferred lines.

nents. For lines not included in the subset $i \notin \mathscr{L}^{\omega}$ —i.e., lines not connected to both busbars—the value of $\phi_{i,l}^{\omega}$ is as previously discussed (i.e., components in series). The presence of these disconnect switches is instrumental in ensuring the reliability and functionality of the DB substation, as demonstrated in Eq. (10), highlighting their crucial role in maintaining overall system performance. A similar approach can be followed for other configurations with built-in redundancies by identifying the series and parallel relationships between components within each line.

4.2.2. Short circuit clearance failures

The second failure mode considered in this study is the short-circuit clearance failure, where the disconnect switches and circuit breakers play a critical role. When a current or potential transformer fails, it triggers a short-circuit failure due to non-operational measurements and temporary overvoltage caused by porcelain breakage, leading to insulation loss through ground contact [62,63]. Disconnect switches and circuit breakers are used to isolate the damaged circuits from the rest of the substation, preventing current flow to the substation busbars, which would otherwise result in a complete substation outage.

The specific components required to clear the short-circuit fault depend on the type of line. For instance, if this fault occurs on an in-line, at least one disconnect switch or circuit breaker downstream of the fault must be operational to clear the fault. If this fault occurs on a transformation line, all upstream and downstream disconnect switches or circuit breakers must be evaluated, requiring that at least one is operational in each case to clear the fault. Finally, if this fault occurs on an out-line, at least one upstream disconnect switch or circuit breaker should be operational to clear this type of fault. Thus, the short-circuit fault corresponds to a series combination of the possibility that a fault could occur in each one of the systems (i.e., in-, transformation, or out-line) and in each one of its lines, as Eq. (11) demonstrates:

$$\Lambda_{s} = \prod_{d=1}^{|I|} \phi_{d,s}^{I} \prod_{h=1}^{|T|} \phi_{b,s}^{T,\text{up}} \cdot \phi_{b,s}^{T,\text{down}} \prod_{k=1}^{|O|} \phi_{k,s}^{O}$$
(11)

where $\phi^I_{d,s}$, $\phi^T_{b,s}$, and $\phi^O_{k,s}$ correspond to the structure functions of short circuit faults related to the d-th in-line, b-th transformation line, and k-th out-line, respectively, with the subscript s indicating that it is associated with short circuit clearance failures. Note that the transformation lines have double the number of structure functions than lines because the short circuit fault can occur either upstream or downstream. The calculation method for the structure function of this fault varies depending on whether the upstream or downstream condition is being considered. To account for this, the elements of the state vector of components \mathbf{x} is classified into two categories depending on the type of component it represents: $\mathbf{x}^{(1)}$ for current or potential transformers, and $\mathbf{x}^{(2)}$ for disconnect switches and circuit breakers. Eq. (12) provides the specific calculation for each case.

$$\phi_{d,s}^{I} = 1 \leftrightarrow \forall x_{n}^{(1)} = 0 \exists x_{m}^{(2)} = 1 \ m > n \ \forall d \in I$$

$$\phi_{b,s}^{T,\text{up}} = 1 \leftrightarrow \forall x_{n}^{(1)} = 0 \ \exists x_{m}^{(2)} = 1 \ m < n \ \forall b \in T$$

$$\phi_{b,s}^{T,\text{down}} = 1 \leftrightarrow \forall x_{n}^{(1)} = 0 \ \exists x_{m}^{(2)} = 1 \ m > n \ \forall b \in T$$

$$\phi_{b,s}^{L,\text{down}} = 1 \leftrightarrow \forall x_{n}^{(1)} = 0 \ \exists x_{m}^{(2)} = 1 \ m < n \ \forall k \in O$$

$$(12)$$

4.3. Functionality and fragility of a substation

Naturally, estimating the functionality of a substation after an earthquake requires evaluating both line faults and short-circuit clearance faults. These failure modes depend on different factors, such as the substation layout, the number and type of internal components, and the number of in-lines, transformation lines, and out-lines. Hence, the exact mathematical expression varies depending on the substation being studied. The functionality of the single busbar (SB), single + transfer

busbar (TB) and double busbar (DB) layouts is given by Eq. (13), which combines in series both types of faults previously described.

$$\Lambda^{\text{SB,TB,DB}} = \prod_{\omega \in \{I,T,O\}} \Lambda_{l}^{\omega} \cdot \Lambda_{s} = \prod_{\omega \in \{I,T,O\}} \left(\frac{1}{|\omega|} \sum_{i=1}^{|\omega|} \phi_{i,l}^{\omega} \right) \cdot \prod_{d=1}^{|I|} \phi_{d,s}^{I}$$

$$\cdot \prod_{k=1}^{|T|} \phi_{b,s}^{T,\text{up}} \phi_{b,s}^{T,\text{down}} \cdot \prod_{k=1}^{|O|} \phi_{k,s}^{O} \tag{13}$$

Substations with a tap off (TO) layout, as previously explained, only feature out-lines. Thus, their functionality is given by Eq. (14).

$$\Lambda^{\text{TO}} = \prod_{\omega \in \{O\}} \Lambda_l^{\omega} \cdot \Lambda_s = \prod_{\omega \in \{O\}} \left(\frac{1}{|\omega|} \sum_{i=1}^{|\omega|} \phi_{i,l}^{\omega} \right) \cdot \prod_{k=1}^{|O|} \phi_{k,s}^{O}$$
(14)

Given the complexity of Eqs. (9)-(14), particularly due to the considerable variability of components in each line and the number of lines in each system, obtaining an analytical solution is not straightforward. Thus, a numerical approach is employed by means of a Monte Carlo simulation. Conceptually, the Monte Carlo simulation estimates the system's performance through a two-step process that is repeated many times for each PGA level. In the first step (Component-Level Sampling), the binary state (1 for operational, 0 for failed) of every individual component in the substation is determined by sampling against its specific fragility curve. In the second step (System-Level Evaluation), this complete set of component states is propagated through the system's logic—as defined by the fault trees and structure functions (Eqs. 9-14)—to calculate a single, deterministic functionality score for the entire substation for that specific simulation. By repeating this process, we build a statistical distribution of the substation's functionality at a given PGA, which is the core of the fragility assessment. The procedure is explained in detail next.

To build the fragility functions of a substation, the Monte Carlo simulation scheme is performed at different levels of ground shaking. This process is summarized in Fig. 10 and can be divided into five steps. First, the components and internal layout of the substation are identified from single-line diagrams, categorizing the lines into the three types, and the components by voltage level (i.e., medium, high, and extrahigh). Second, a wide range of values of the ground motion intensity measure, defined here as the peak ground acceleration (PGA), is selected. The range spans from 0 g to 2.0 g in increments of 0.01 g, which was determined to be sufficient to capture the entire spectrum of substation performance—from near-zero failure probability to near-certain failure—thereby ensuring that the resulting fragility functions are welldefined over their full range. Third, and for each PGA value, the operational states of all components are sampled using N = 1,000 Monte Carlo simulations. This sample size was selected based on a preliminary convergence study, which indicated that 1,000 simulations provide stable estimates of the failure probabilities. Larger sample sizes were found to yield negligible changes to the final fragility function parameters (median and logarithmic standard deviation), confirming the adequacy of this choice. Fourth, the component states are used to evaluate the operational state of each line and possible short circuit failures, which in turn are used to evaluate the operational state of the substation based on the previously identified internal layout, specifically, the proportion of the substation that remains functional. These proportions are compared to a given functionality threshold to estimate the probability of exceeding the threshold as the number of exceedance cases divided by the total number of simulations (N). Finally, a fragility function is fitted to these probabilities at all PGA values using maximum likelihood estimation. This process yields fragility functions for the substation representing limit states comparable to those presented in HAZUS, which represent 5 %, 40 %, 70 %, and 100 % of damage. However, in this study, the focus is on the percentage of the overall functionality of the substation that is lost rather than the percentage of damaged components, as done in HAZUS.

The proposed method is computationally efficient for large-scale

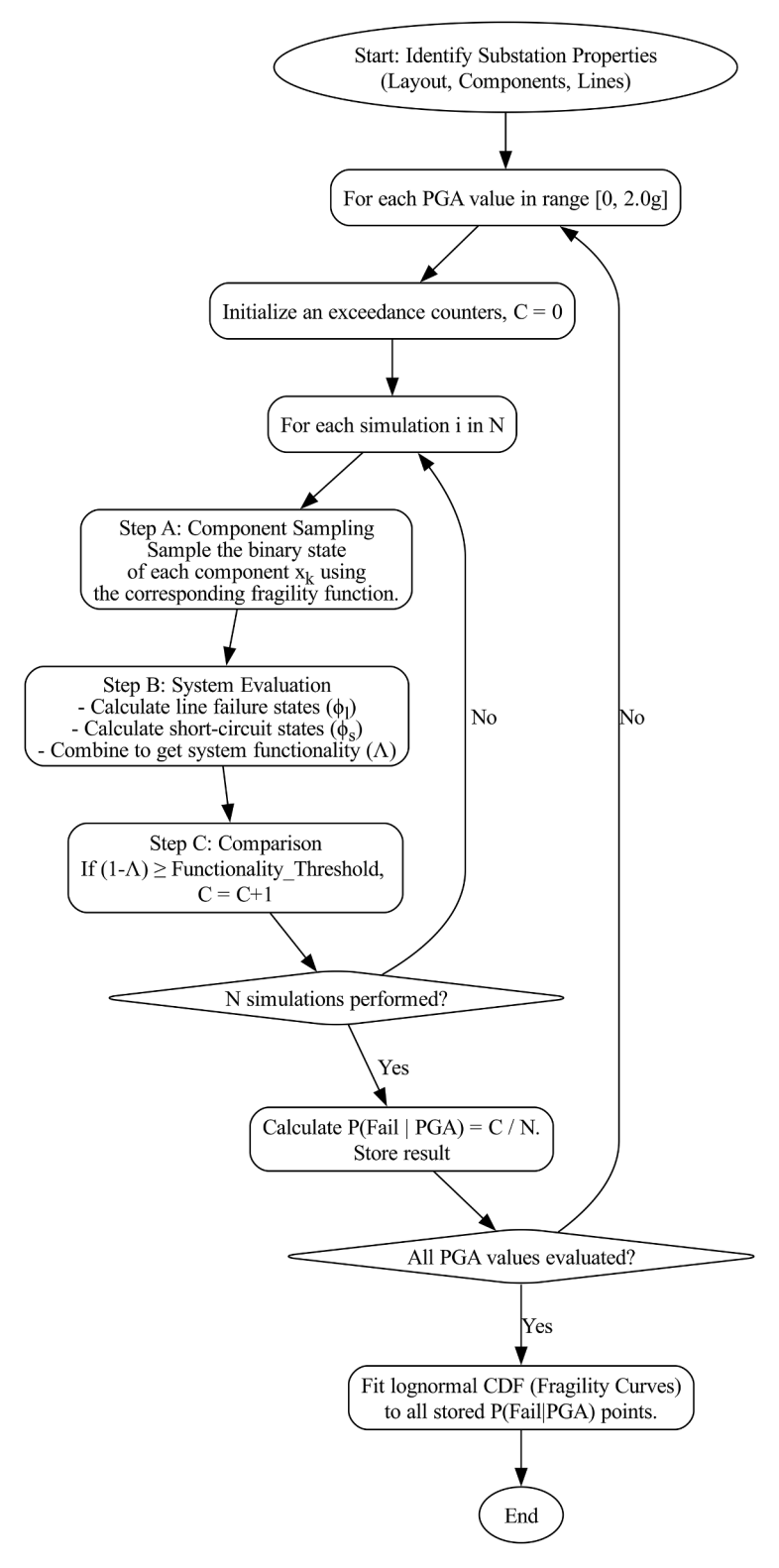


Fig. 10. Flowchart for estimating the seismic fragility of a substation.

applications, with single-substation analyses completing in few minutes. The framework is inherently scalable and parallelizable due to the independent nature of each simulation. While future optimizations such as variance reduction techniques are possible, the current performance proved sufficient for analyzing the 1100 substation portfolio in this study.

The method described above assumes that component failures are

conditionally independent events given the ground motion intensity measure. However, there are some phenomena that could introduce correlations between components failures, such as common construction practices and materials. To quantify the impact of this simplifying assumption, a sensitivity analysis was performed on a representative, complex substation archetype. Two bounding scenarios were modeled: (1) the baseline conditional independence case (ρ =0), used in this study;

and (2) perfect correlation by component type (ρ =1), an upper-bound scenario in which all components of the same type fail or operate together. The results of this analysis (see Figure S13 in Supplementary Material) show that failure correlation alters the system's fragility by collapsing the fragility curves for all functionality loss states into a single curve with higher dispersion, lying between the slight and complete functionality loss states. This indicates a brittle system behavior, where the substation transitions directly from a largely operational state to complete failure. The true fragility of the system may lie between these two bounding behaviors, and its characterization would require more refined models of the correlation structure.

4.4. Example substation fragility computation

To illustrate the method described above, the example electric power substation represented by the single-line diagram of Fig. 11a is used. The substation corresponds to a single busbar configuration with two inlines, one transformation line, and two out-lines. Each in-line consists of three components in series, namely, a potential transformer (PT1 and PT2), a disconnect switch (Dis1 and Dis2), and a circuit breaker (CB1 and CB2). The transformation line consists of seven components in series: two disconnect switches (Dis3 and Dis4), two current transformers (CT1 and CT2), two circuit breakers (CB3 and CB4), and one power transformer (T2D1). Each out-line consists of three components in

series, namely, a disconnect switch (Dis5 and Dis6), a circuit breaker (CB5 and CB6), and a current transformer (CT3 and CT4). Additionally, the substation has two bus bars (BusBar1 and BusBar2) of different voltage levels.

The fault trees shown in Fig. 11b and c detail all the line and short circuit clearance fault cases for this example substation, respectively. The former type of fault requires disconnect switches, circuit breakers, and power transformers to be operational for complete functionality of the electrical substation, whereas the latter type of fault requires disconnect switches or circuit breakers to be operational in case of a potential or current transformer failure. Within each fault tree, out-of-service components are depicted by red circles that are interconnected through AND and OR logic gates. Additionally, each Fault Event (FE) is represented by white rectangles with its respective structure function.

As depicted in Fig. 11b, the fault events FEC1, FEC2, FEC3, FEC4, and FEC5 align with line failure cases associated to structure functions $\phi_{1,l}^I$, $\phi_{2,l}^I$, $\phi_{1,l}^T$, $\phi_{1,l}^O$, $\phi_{2,l}^O$, respectively. In Fig. 11c, the fault events FESC1, FESC3, FESC3, FESC4, FESC5, and FESC6 correspond to short circuit failures and are linked to structure functions $\phi_{1,s}^I$, $\phi_{2,s}^I$, $\phi_{1,s}^{T,up}$, $\phi_{1,s}^{T,down}$, $\phi_{1,s}^O$, and $\phi_{2,s}^O$. The structure functions are then combined using Eq. (13) to obtain the state of the substation, which corresponds to the proportion that remains functional. One minus this value corresponds to the proportion of the substation that is not operational (F):

$$F = 1 - \Lambda^{SB}$$

$$= 1 - \left[\left(\frac{1}{2} \sum_{i=1}^{2} \phi_{i,l}^{I} \right) \left(1 \sum_{i=1}^{1} \phi_{i,l}^{T} \right) \left(\frac{1}{2} \sum_{i=1}^{2} \phi_{i,l}^{O} \right) \right] \left[\left(\prod_{d=1}^{2} \phi_{d,s}^{I} \right) \left(\prod_{b=1}^{1} \phi_{b,s}^{T,\text{down}} \right) \left(\prod_{k=1}^{2} \phi_{k,s}^{O} \right) \right]$$

$$= 1 - \left[\left(\frac{\phi_{1,l}^{I} + \phi_{2,l}^{I}}{2} \right) \cdot \left(\frac{\phi_{1,l}^{T} + \phi_{2,l}^{O}}{2} \right) \right] \cdot \left[\left(\phi_{1,s}^{I} \phi_{2,s}^{I} \right) \left(\phi_{1,s}^{T,\text{down}} \phi_{1,s}^{T,\text{down}} \right) (\phi_{1,s}^{O} \phi_{2,s}^{O}) \right]$$

$$(15)$$

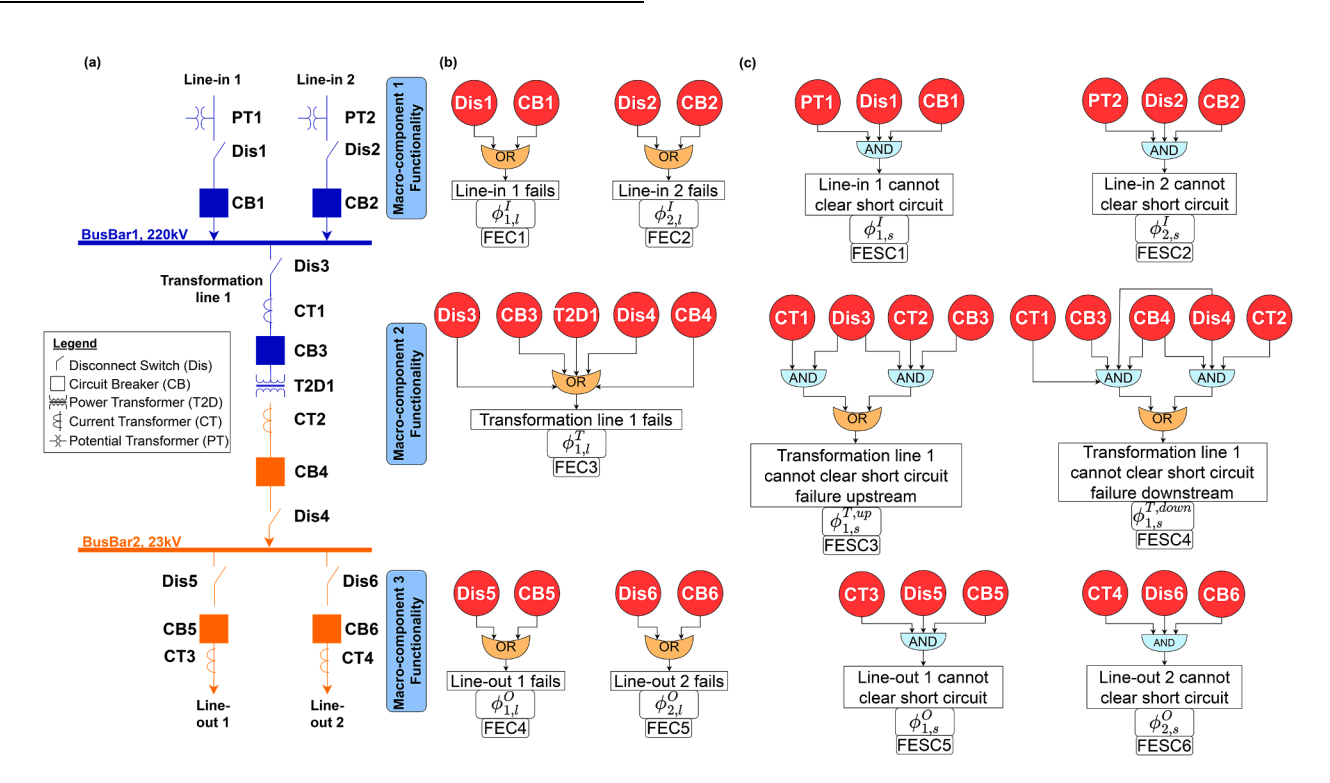


Fig. 11. Example substation with a single busbar layout. (a) Single-line diagram, (b) fault trees of the line failure cases, and (c) fault trees of the short circuit clearance failure cases.

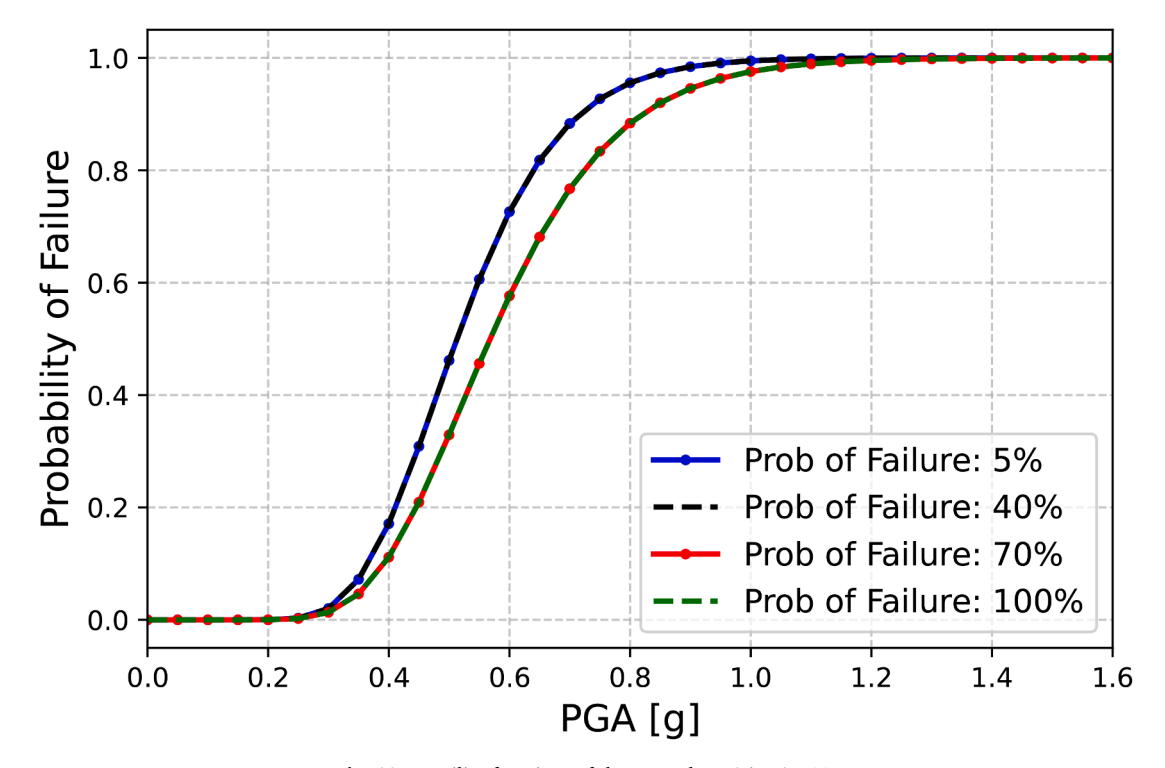


Fig. 12. Fragility functions of the example EPS in Fig. 11.

The proportion of Eq. (15) was evaluated for 1,000 simulations for each PGA value and compared to the 5 %, 40 %, 70 %, and 100 % thresholds defined by HAZUS. Fig. 12 presents the fragility functions fitted for the example substation, illustrating the probability of exceeding these thresholds at various levels of peak ground acceleration (PGA). The curves indicate that the probability of exceeding the 5 % and 40 % damage states is identical, as is the case for the 70 % and 100 %

damage states. This phenomenon occurs because of the limited number of in-, transformation, and out-lines in the example substation, which leads to the functionality only changing by multiples of 25 %.

5. Substation fragility functions

Fragility functions were computed for each substation in Chile using damage states similar to those defined by HAZUS. However, instead of focusing on the number of failed components, as done by HAZUS, the

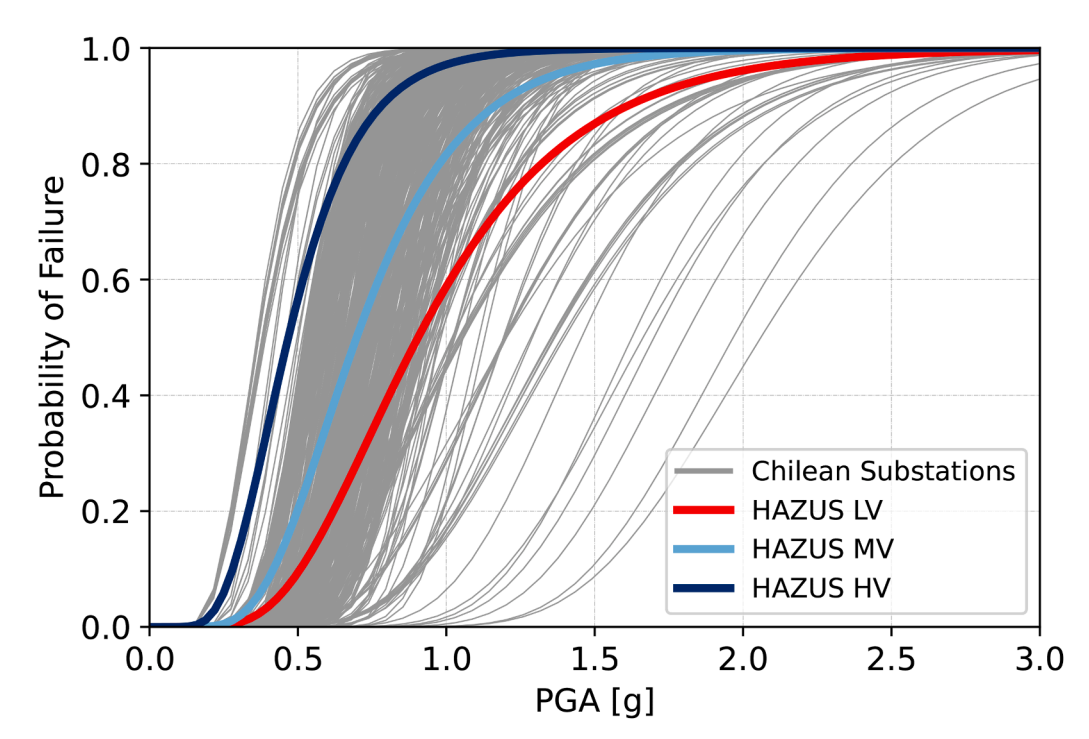


Fig. 13. Fragility functions of all Chilean Substations and those of HAZUS for three voltage levels. All fragility functions correspond to the Complete damage state.

approach used here evaluates system functionality based on the same percentage thresholds. These calculations accounted for the internal configuration of the substations, the types and characteristics of the internal components, and their behavior under seismic loads. Using the component fragility functions from Section 3 and the novel approach outlined in Section 4, fragility functions were developed for each of the 1100 substations.

Fig. 13 shows the fragility functions for individual substations and the corresponding HAZUS fragility functions for low-, medium-, and high-voltage substations in the complete damage state. The individual substation curves exhibit significant variability and can differ significantly from the HAZUS curves, suggesting a need for more detailed fragility models that account for the unique characteristics of each substation.

5.1. Clustering of fragility functions

To obtain general results that are easier to use, fragility functions were classified into a reduced number of archetypes. The classification was carried out by a recursive algorithm that generates a decision tree based on the following substation properties: voltage level (first divisive variable), internal layout; and number of in-, transformation-, and outlines. The algorithm is an adaptation of the one used elsewhere [64], which can consider continuous, integer, and categorical properties simultaneously. At each step, the algorithm divides a group of curves into two subgroups by selecting the substation property and value that minimizes the variability of the resulting subgroups. Variability is defined with a statistical technique employed to normalize the dispersion of data by dividing the range (i.e., the difference between the maximum and minimum value) by the mean of the dataset. This normalization process is particularly useful when comparing datasets with varying scales or when the magnitude of the values is less relevant than the relative spread. The method is used as part of a fitness function to evaluate the quality of different data splits. The fitness function evaluates the variability of the two key features of the dataset using a

statistical technique based on the median and logarithmic standard deviation of the fragility function. Specifically, the function assigns weights of 1 to the median and 0.5 to the logarithmic standard deviation, giving greater importance to the first feature. These weighted values are combined to compute the overall measure of variability. The optimization algorithm then identifies the split that minimizes the weighted combination of these statistical measures. By doing so, the fitness function ensures that the selected partition achieves the lowest possible variability while balancing the relative importance of each feature. Additionally, the function evaluates all candidate partitions to ensure that the subgroup with the worst-case (maximum) normalized range is minimized, thus promoting homogeneous subgroups, as shown in Eq. (16).

$$F(x) := \min(\max(w^T \cdot \widehat{r}_1(x), w^T \cdot \widehat{r}_2(x)))$$
(16)

Vectors \hat{r}_1 and $\hat{r}_2 \in \mathbb{R}^2$ have the ranges of the parameters, normalized by their mean value, of the two potential subgroups, where the first and second components correspond to the median and the logarithmic standard deviation of the fragility function, respectively. Additionally, $w = [1, 0.5]^T$ is a weight vector that assigns different levels of importance to the parameters. Depending on the problem's size, an exhaustive search or a heuristic method is employed to evaluate all possible divisions. The process continues for each subgroup until the variance is below a certain tolerance value, the number of curves in the subgroup is low enough, or the maximum tree depth is reached. The algorithm was used independently for each substation layout considering a maximum tree depth of 3, a tolerance of 0.01, and 5 as a minimum number of curves per group, except for the single busbar layout, where a minimum value of 15 curves was considered. Moreover, the initial decision variable was forced to be the voltage level to ease the interpretation of results and align with industry-standard classifications (e.g., HAZUS), as voltage is a primary factor governing component design and performance. A sensitivity analysis, detailed in the Supplementary Material to this article (Figure S15), shows that the resulting archetypes are highly stable to variations of these weights.

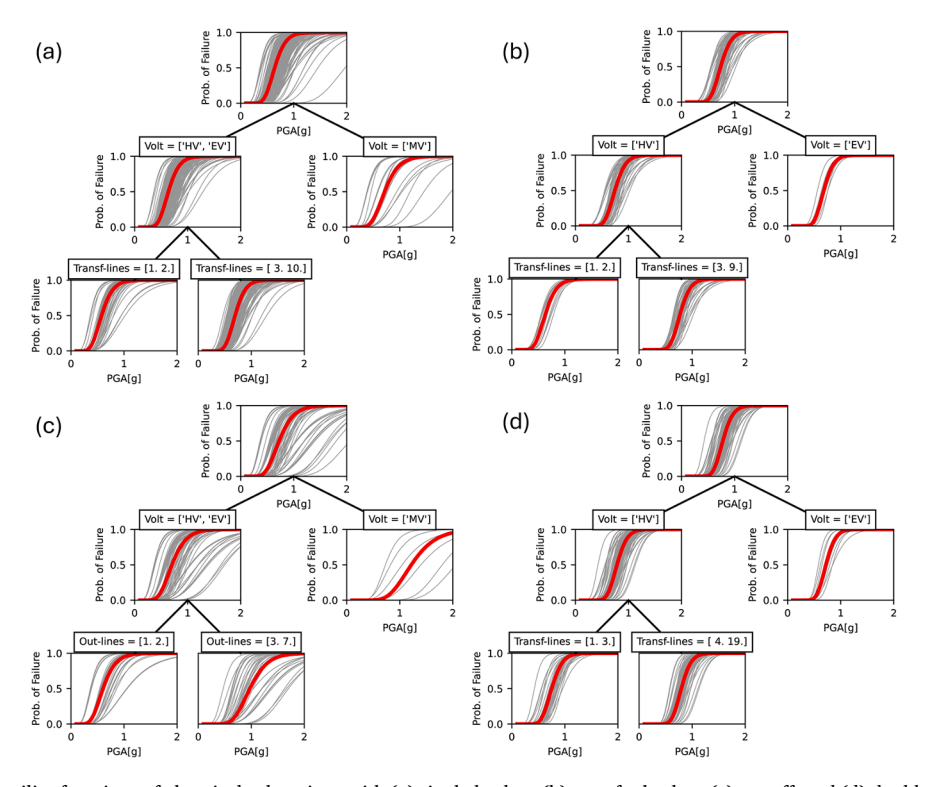


Fig. 14. Classification of fragility functions of electrical substations with (a) single busbar, (b) transfer busbar, (c) tap off, and (d) double busbar layout, for the case of components with 2 % damping.

Table 2Estimated parameters of substation archetype fragility functions for complete damage state.

Layout	Elements in cluster	Voltage level	Transformation lines	Out-lines	$\xi = 2\%$		$\xi=1\%$		$\xi = 0.5\%$	
					θ	β	θ	β	θ	β
Single busbar	169	HV-EV	1–2	_	0.58	0.29	0.52	0.26	0.49	0.26
Single busbar	194	HV-EV	3–10	_	0.70	0.22	0.60	0.21	0.55	0.21
Single busbar	18	MV	_	_	0.72	0.30	0.67	0.27	0.62	0.28
Transfer busbar	12	HV	1–2	_	0.63	0.27	0.55	0.25	0.52	0.25
Transfer busbar	50	HV	3–9	_	0.77	0.20	0.64	0.19	0.55	0.19
Transfer busbar	8	EV	_	_	0.68	0.21	0.59	0.19	0.55	0.19
Double busbar	28	HV	1-3*	210^{\dagger}	0.75	0.21	0.64	0.20	0.60	0.21
Double busbar	76	HV	4–19*	$11-29^{\dagger}$	0.79	0.18	0.62	0.19	0.57	0.20
Double busbar	8	EV	_	_	0.72	0.18	0.60	0.20	0.54	0.21
Tap off	82	HV-EV	_	1–2	0.61	0.31	0.53	0.30	0.50	0.30
Tap off	39	HV-EV	_	3–7	0.98	0.27	0.79	0.25	0.74	0.25
Tap off	6	MV	-	_	1.22	0.30	1.13	0.26	0.99	0.27

^{*} For the double busbar layout, transformation lines are only valid for the 2 % damping case.

The decision trees that resulted from the 2 % damping cases and the complete damage state are presented in Fig. 14, with the final archetypes for each substation layout defined by each end-node of the trees. These archetypes and the parameters of their associated fragility functions for different damping ratios ($\xi = 2$ %, 1 %, and 0.5 %) are presented in Table 2. Each row in the table corresponds to an archetype, defined by its voltage level, number of transformation lines, and number of out-lines. Since multiple fragility functions exist within each archetype, their parameters were averaged to derive a single representative fragility function that reflects the typical behavior of the archetype. These parameters, which correspond to the median (θ) and logarithmic standard deviation (β) of the PGA that produces complete damage (see Eq. (3)), are also provided in Table 2. Note that the transfer busbar and the double busbar archetypes do not consider medium voltage as these combinations do not exist in the database of Chilean substations. The same analysis was repeated for the other damage states defined by HAZUS (i.e., slight, moderate, and extensive), with the results shown in Tables S1, S2, and S3 of the supplementary material to this article.

The resulting fragility functions for complete damage state and $2\,\%$ damping with medium, high, and extra high voltages are shown in Figs. 15a, 16, and Fig. 15b, respectively. In general, archetypes of the tap off layout tend to be less fragile than those of other layouts. The figures also show that the archetypes tend to be more fragile as the voltage level increases. Results for the rest of the damage states are presented in Figures S1-S6 of the supplementary material to this article.

Fig. 17 depicts the effect of the damage state and damping ratio on the fragility functions of the two archetype single busbar substations with high voltage. Fig. 17a shows how fragility functions that consider a damping ratio of 2% change with the damage state, whereas Fig. 17b shows how fragility functions for the Complete damage state become

more fragile as the damping ratio decreases. Similar results were obtained for the rest of the substation configurations and are presented in Figures S7-S9 in the supplementary material to this article.

5.2. Discussion of factors influencing substation fragility

The results reveal that substation fragility is sensitive to several key input parameters at both the component and system levels. A sensitivity analysis was performed on the component damping ratio, as this parameter is subject to uncertainty and has a strong influence on the dynamic response. As shown in Fig. 17b, the final substation fragility is highly sensitive to the assumed damping. Lower damping values, which may be more representative of real-world conditions than the 2 % value mandated by some design codes, lead to significantly higher probabilities of failure for the same level of ground shaking. This is because reduced damping increases the dynamic amplification of the components' response, leading to higher stresses on critical porcelain elements and a more vulnerable system overall. This finding underscores the importance of accurately characterizing component damping in substation fragility assessments. Additionally, higher voltage levels necessitate larger components with greater mass and an elevated center of gravity. This design results in larger inertial forces and overturning moments during an earthquake, increasing component stress and overall substation vulnerability. At the system level, the internal layout is a primary driver of variability. For instance, Tap Off layouts prove less fragile because their simpler operational model as defined in this study (Eq. (14)) involves fewer failure pathways than more complex configurations like the Single Busbar (Eq. (13)), which integrates three distinct subsystems.

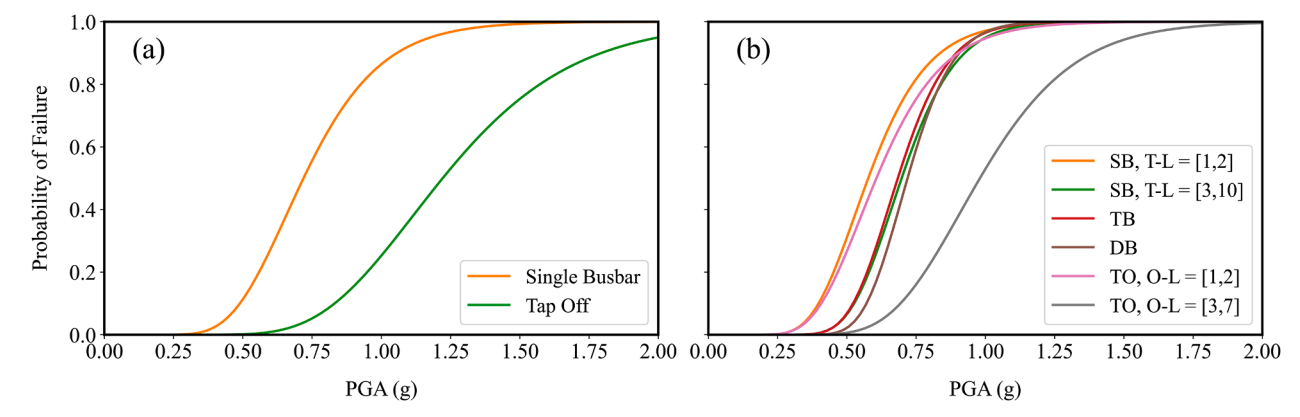


Fig. 15. Fragility functions for complete damage state of archetype substations and $\xi=2$ % of damping, with: (a) medium voltage and (b) extra high voltage.

For the double busbar layout, out-lines are only valid for the 1 % and 0.5 % damping cases.

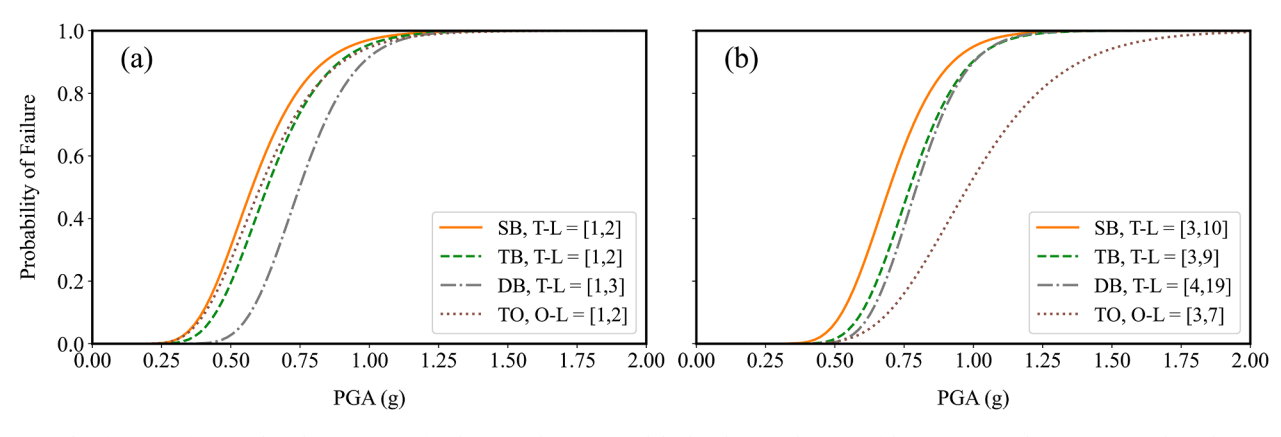


Fig. 16. Fragility functions for complete damage state of archetype substations with high voltage and ξ=2 % of damping: (a) archetypes type 1, (b) archetypes type 2.

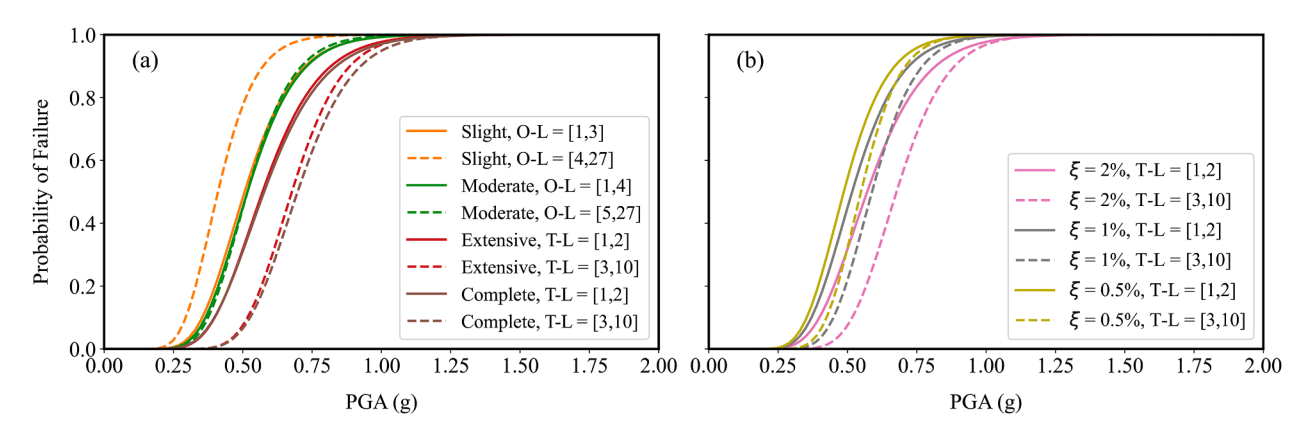


Fig. 17. Fragility functions for single busbar archetypes in extra high and high voltage: (a) different damage states considering 2 % damping and (b) complete damage state and different damping ratios.

Table 3Estimated parameters of substation archetype fragility functions for complete damage state using HAZUS voltage levels.

Layout	Elements in cluster	Voltage level	Transformation lines	Out-lines	$\xi=2\%$	
					θ	β
Single busbar	60	MV-HV	1–2	_	0.56	0.28
Single busbar	87	MV-HV	3–10	_	0.67	0.21
Single busbar	234	LV	_	_	0.65	0.26
Transfer busbar	33	HV	_	_	0.64	0.20
Transfer busbar	32	MV	_	_	0.73	0.19
Transfer busbar	3	LV	_	_	0.75	0.23
Double busbar	13	MV-HV	1–2	=	0.78	0.21
Double busbar	66	MV-HV	3–11	_	0.79	0.18
Double busbar	33	LV	_	_	0.76	0.20
Tap off	13	HV	_	_	0.38	0.35
Tap off	47	MV	_	_	0.68	0.29
Tap off	67	LV	_	-	0.85	0.30

5.3. Comparison with existing substation fragility functions

To enable a fair comparison with HAZUS substation fragility functions, the substations were regrouped following the HAZUS voltage ranges (i.e., low, medium, and high), which differ from the Chilean voltage ranges used in this study. The same clustering procedure was then followed to obtain archetypes with representative fragility function parameters. Table 3 presents the resulting archetypes for the case of complete damage state and 2 % damping, and their associated fragility functions are compared to those of anchored components from HAZUS in Fig. 18. Similar results for the rest of the damage states are presented in Tables S4-S6 and Figures S10-S12 of the supplementary material to

this article. While the HAZUS curves for the medium voltage level fall near the center of the proposed archetypes, significant deviations are observed for other cases. These discrepancies are not arbitrary but stem from fundamental differences in modeling philosophy.

The most critical distinction is that our model defines failure based on system-level functionality, which is intrinsically linked to the substation's specific internal layout. In contrast, the generic HAZUS methodology defines damage states based on the percentage of physically broken components, without considering their topological arrangement. Our approach, therefore, captures scenarios that a component-counting method cannot; for example, the failure of a single critical upstream component can lead to a 100 % loss of functionality, while significant

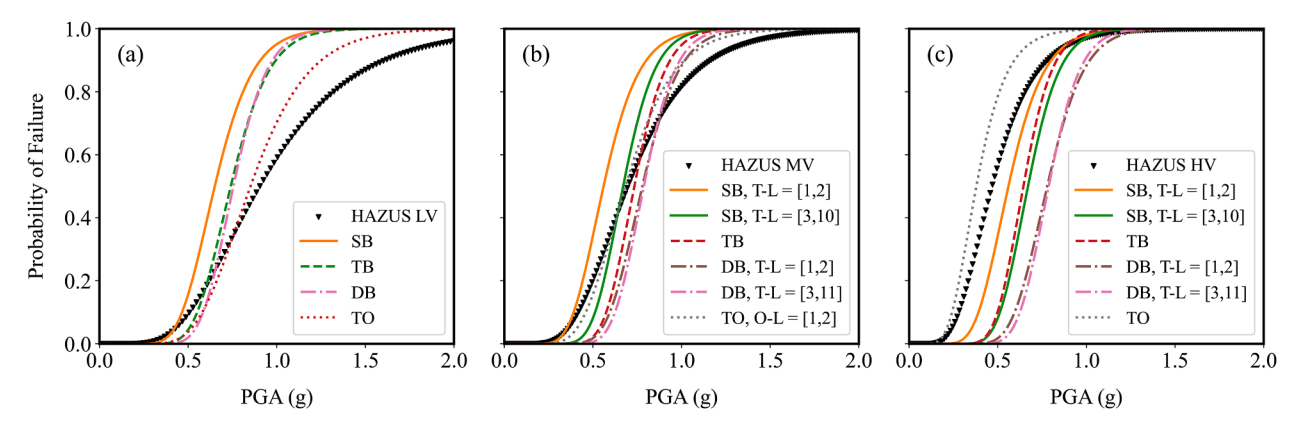


Fig. 18. Comparison between the proposed substation archetype fragility functions considering 2 % damping and complete damage state (i.e., total loss of functionality) with those of HAZUS for (a) low, (b) medium, and (c) high voltages. Discrepancies are driven by the proposed model's use of a layout-specific, functionality-based failure metric versus the generic, component-damage-based approach of HAZUS.

redundancy in other layouts can maintain power flow despite multiple component failures.

Furthermore, the fragility inputs differ. The components modeled in this study were designed according to modern and stringent Chilean seismic codes, which can result in higher seismic resistance compared to the broader, and potentially older, equipment inventory represented in the generic HAZUS functions. Our model also incorporates systemic failure modes, such as short-circuit clearance faults, that can disable an entire substation and are not explicitly captured in the HAZUS framework. Excluding this failure mechanism leads to a systematic overestimation of the median capacity (θ) of the fragility functions. For the complete damage state, the average overestimation is 3.6 % across the substations in this study, but it can exceed 30 % for some substations. The Supplementary Material provides a statistical representation of this overestimation (Table S7 and Figure S14). The interplay of these factors—a stricter functionality-based failure definition applied to often more robust components and layouts-explains the significant and varied differences observed in Fig. 18.

6. Summary and conclusions

This study presents a novel method to estimate the fragility of 1,100 electrical substations based on the configuration and seismic performance of their internal components. Multiple stripe analyses are first used to construct seismic fragility functions of the internal components. The functionality of a substation is then constructed based on the damage to these components, which can result in individual lines within the substation losing their functionality or in short circuit faults that render the complete substation nonfunctional. Both types of faults are modeled using fault trees and are combined depending on the internal configuration of the substations. Finally, the functionality of the substation is sampled using Monte Carlo simulation to obtain seismic fragility curves.

The method was applied to estimate the fragility functions of substations of the Chilean electrical power grid, specifically focusing on the four most common layouts found in the country (single busbar, single and transfer busbar, double busbar, and tap off). The resulting fragilities vary significantly with the internal configuration of the substations, the voltage level of components, and with some modeling choices, especially the damping ratio considered for the dynamic analysis of substation components. To ease the use of the computed fragility functions, they were then clustered in several substation archetypes that are defined based on their internal component layouts, voltage levels, and number of lines.

The fragility functions vary significantly between the archetypes and with those provided by HAZUS, which are not dependent on the internal configuration of substation components. These results suggest that the

fragility characterization of substations can be improved significantly by considering a model tailored to regional-specific substation configurations. The significant discrepancies revealed between the proposed fragility functions and the generic curves from HAZUS underscore the value of this tailored approach for improving seismic risk characterization. By moving beyond generic models to account for specific internal configurations, the proposed method enables more accurate and reliable risk and resilience analyses. This has direct, practical implications for enhancing power system resilience. For example, utility operators can use these specific fragility models to inform risk-based decision-making, such as prioritizing seismic retrofitting for the most vulnerable substation archetypes or optimizing hardening strategies by targeting critical components within a specific layout. The methodology can also guide the design of new substations, allowing for the proactive selection of internal configurations that minimize seismic fragility from the outset. On a broader scale, this type of layout-specific analysis could supplement or replace generic approaches in regional assessment standards and, conceptually, serve as a model for evaluating the seismic resilience of other critical lifeline systems.

Finally, it is important to acknowledge the limitations of this study, which in turn suggest avenues for future research. First, while the case study focused on the four most relevant layouts for the Chilean grid, the proposed methodology is generic and can be extended to other configurations (e.g., breaker-and-a-half, ring bus) to increase its international applicability. Second, the fragility functions developed herein are based on numerical simulations and have not been validated against empirical damage data from past earthquakes. Performing such a validation is a recognized challenge due to the scarcity of detailed, component-level post-earthquake data, but it remains a critical step for future work to enhance the credibility of the models. Third, the structural models in SAP2000 were developed using deterministic geometric and material properties. This approach does not capture the inherent aleatory uncertainty in these parameters. Future studies could address this by incorporating this variability into the analysis, A robust method would involve sampling key material and geometric properties from appropriate probability distributions and propagating these uncertainties through the dynamic simulations. This would provide a more rigorous basis for the resulting fragility curve parameters (both median, θ , and dispersion, β). Fourth, the component failure criterion was based on a uniform safety factor of 2.0 derived from local design codes. Although our validation against established literature shows this approach yields reasonable results for a system-level study, this simplification does not capture the unique, physics-based failure modes of each component. Future research should aim to integrate more granular, componentspecific failure criteria (e.g., strain limits in porcelain, bushing oil leakage) as more detailed experimental data becomes available. Fifth, while this study assessed the sensitivity of the results to component damping, a more comprehensive sensitivity analysis was beyond the current scope. Future work could systematically investigate the influence of other key sources of uncertainty, such as the dispersion (β) of the component fragility curves and the effect of site-specific ground motion characteristics (e.g., soil type and location), to further understand the robustness of the results. Sixth, the primary analysis assumed conditional independence between component failures given a ground motion intensity, which is a simplification. A sensitivity analysis was performed to quantify the impact of this assumption, showing that failure correlation can influence system vulnerability and lead to more brittle responses. A more refined model of the partial correlation structure between component failures could be a critical topic for future research.

Funding

This work was supported by the Research Center for Integrated Disaster Risk Management (CIGIDEN) ANID/FONDAP/1523A0009, and the research grant "Multiscale earthquake risk mitigation of healthcare networks using seismic isolation" ANID/FONDECYT/1220292, both funded by the National Agency for Research and Development (ANID). The authors are grateful for this support.

CRediT authorship contribution statement

Nicolás Ahumada: Writing – review & editing, Writing – original draft, Visualization, Validation, Software, Resources, Methodology, Investigation, Formal analysis, Data curation, Conceptualization. Juan Pablo Muñoz Gálvez: Writing – review & editing, Writing – original draft, Visualization, Software, Resources, Project administration, Methodology, Formal analysis, Conceptualization. Alan Poulos: Writing – review & editing, Writing – original draft, Visualization, Methodology, Félix Rojas: Writing – review & editing, Validation, Methodology, Conceptualization. Juan Carlos de la Llera: Writing – review & editing, Supervision, Project administration, Methodology, Funding acquisition, Conceptualization.

Declaration of competing interest

The authors declare that they have no known competing financial interests or personal relationships that could have appeared to influence the work reported in this paper.

Acknowledgements

The strong motion database was provided by the SIBER-RISK project: Simulation Based Earthquake Risk and Resilience of Interdependent Systems and Networks ANID/ FONDECYT/1170836. https://doi.org/10.7764/datasetUC/ING-UC.11708361.

Supplementary materials

Supplementary material associated with this article can be found, in the online version, at doi:10.1016/j.ress.2025.111671.

Data availability

Data will be made available on reasonable request.

References

- [1] Panteli M, Mancarella P. The grid: stronger, bigger, smarter? IEEE Power Energy Mag 2015:58–66. https://doi.org/10.1109/MPE.2015.2397334.
- [2] Lin JH, Wu YK. Review of power system resilience concept, assessment, and enhancement measures. Appl Sci 2024;14(4). https://doi.org/10.3390/ app14041428.

- [3] Huang X, Wang N. Post-disaster restoration planning of interdependent infrastructure systems: a framework to balance social and economic impacts. Struct Saf 2024;107:102408. https://doi.org/10.1016/J.STRUSAFE.2023.102408.
- [4] Liu R, Zhang MJ, Wu YB. Vulnerability study of electric power grid in different intensity area in Wenchuan earthquake. In: 15th World Conf. Earthq. Eng. (WCEE); 2012
- [5] Oral B, Dönmez F. The impacts of natural disasters on power systems: anatomy of the marmara earthquake blackout. Acta Polytech Hungarica 2010;7(2):107–18.
- [6] J.C. Araneda, H. Rudnick, and S. Mocarquer, "Lessons from the 2010 Chilean earthquake and its impact on electricity supply," no. Powercon, pp. 1–7, 2010.
- [7] Sordo S, Domaneschi M, Cimellaro GP, Mahin S. Seismic resilience of electric power networks in urban areas. In: Maintenance, Safety, Risk, Manag. Life-Cycle Perform. Bridg. - Proc. 9th Int. Conf. Bridg. Maintenance, Saf. Manag. IABMAS 2018; 2018. p. 1911–9. https://doi.org/10.1201/9781315189390-260.
- [8] NavarroEspinosa A, et al. Improving distribution network resilience against earthquakes. IET Conf Publ 2017;2017(CP727):3–8. https://doi.org/10.1049/ cp.2017.0339.
- [9] Ferrario E, Poulos A, Castro S, de la Llera JC, Lorca A. Predictive capacity of topological measures in evaluating seismic risk and resilience of electric power networks. Reliab Eng Syst Saf 2022;217:108040. https://doi.org/10.1016/j. ress.2021.108040.
- [10] Espinoza S, Poulos A, Rudnick H, De La Llera JC, Panteli M, Mancarella P. Risk and resilience assessment with component criticality ranking of electric power systems subject to earthquakes. IEEE Syst J 2020;14(2):2837–48. https://doi.org/10.1109/ JSYST.2019.2961356.
- [11] Sun X, Feng D, Zhang Q, Lin S. Optimal siting of substations of traction power supply systems considering seismic risk. Reliab Eng Syst Saf 2024;243:109801. https://doi.org/10.1016/J.RESS.2023.109801.
- [12] Liang H, Xie Q. Probabilistic seismic risk analysis of electrical substations considering equipment-to-equipment seismic failure correlations. Reliab Eng Syst Saf 2025;253:110588. https://doi.org/10.1016/J.RESS.2024.110588.
- [13] Oboudi MH, Mohammadi M. Two-stage seismic resilience enhancement of electrical distribution systems. Reliab Eng Syst Saf 2024;241:109635. https://doi. org/10.1016/J.RESS.2023.109635.
- [14] Guo X, Li H, Zhang H. Damage risk assessment of transmission towers based on the combined probability spatial-temporal distribution of strong winds and earthquakes. Reliab Eng Syst Saf 2025;261:111078. https://doi.org/10.1016/J. RESS.2025.111078.
- [15] Liang H. A reliability-based approach to identify critical components in a UHVDC converter station system against earthquakes. Reliab Eng Syst Saf 2025;260: 110977. https://doi.org/10.1016/J.RESS.2025.110977.
- [16] Liang H, Xie Q. Probabilistic seismic risk analysis of electrical substations considering equipment-to-equipment seismic failure correlations. Reliab Eng Syst Saf 2025;253:110588. https://doi.org/10.1016/J.RESS.2024.110588.
- [17] Liu X, Xie Q. A multi-strategy framework to evaluate seismic resilience improvement of substations. Reliab Eng Syst Saf 2024;245:110045. https://doi. org/10.1016/J.RESS.2024.110045.
- [18] Liu X, Xie Q. A probabilistic framework to evaluate seismic resilience of substations based on three-stage uncertainty. Reliab Eng Syst Saf 2024;249:110219. https://doi.org/10.1016/J.RESS.2024.110219.
- [19] FEMA. Hazus Earthquake model technical manual. Fed Emerg Manag Agency 2020:(October):1–436.
- [20] Ang AHS, Pires JA, Villaverde R. A model for the seismic reliability assessment of electric power transmission systems. Reliab Eng Syst Saf 1996;51(1):7–22. https://doi.org/10.1016/0951-8320(95)00101-8.
- [21] Rasulo A, Goretti A, Nuti C. Performance of lifelines during the 2002 Molise, Italy, earthquake. Earthq Spectra 2004;20(SPEC. 1):301–14. https://doi.org/10.1193/ 1.1768542
- [22] Li J, Wang T, Shang Q. Probability-based seismic resilience assessment method for substation systems. Struct Infrastruct Eng 2021;18(1):71–83. https://doi.org/ 10.1080/15732479.2020.1835998.
- [23] Liu X, Xie Q, Liang H, Zhu W. Seismic resilience evaluation and retrofitting strategy for substation system. Int J Electr Power Energy Syst 2023;153(May):109359. https://doi.org/10.1016/j.ijepes.2023.109359.
- [24] Straub D, Der Kiureghian A. Improved seismic fragility modeling from empirical data. Struct Saf 2007;30(4):320–36. https://doi.org/10.1016/j. strusafe.2007.05.004.
- [25] Paolacci F, Giannini R, Alessandri S, De Felice G. Seismic vulnerability assessment of a high voltage disconnect switch. Soil Dyn Earthq Eng 2014;67:198–207. https://doi.org/10.1016/j.soildyn.2014.09.014.
- [26] Wen B, Moustafa MA, Junwu D. Seismic fragilities of high-voltage substation disconnect switches. Earthq Spectra 2019;35(4):1559–82. https://doi.org/ 10.1193/030118EOS049M.
- [27] Moustafa MA, Mosalam KM. Structural performance of porcelain and polymer post insulators in high voltage electrical switches. J Perform Constr Facil 2016;30(5). https://doi.org/10.1061/(asce)cf.1943-5509.0000848.
- [28] Zareei SA, Hosseini M, Ghafory-Ashtiany M. Seismic failure probability of a 400 kV power transformer using analytical fragility curves. Eng Fail Anal 2016;70:273–89. https://doi.org/10.1016/j.engfailanal.2016.09.007.
- [29] Zareei SA, Hosseini M, Ghafory-Ashtiany M. Evaluation of power substation equipment seismic vulnerability by multivariate fragility analysis: a case study on a 420 kV circuit breaker. Soil Dyn Earthq Eng 2017;92(March 2016):79–94. https:// doi.org/10.1016/j.soildyn.2016.09.026.
- [30] Anagnos T. Development of an electrical substation equipment performance database for evaluation of equipment fragilities. PEER Rep 1999;2001/06.

- [31] Pinto PE, Cavalieri F, Franchin P, Vanzi I, Pitilakis K. SYNER-G: deliverable D3.3 fragility functions for electric power system elements. Syner-G Deliv D 2010;3.3:96 [Online]. Available: http://www.vce.at/SYNER-G/pdf/deliverables/D3. 03 SYNER-G Fragility-functions-for-electric-power-system-elements.pdf.
- [32] Mao Y, He C, Jiang L, Lai Z. Seismic fragility of the overhead catenary system on high-speed railway bridges using composite intensity measure classification. Structures 2025;79(May):109578. https://doi.org/10.1016/j.istruc.2025.109578.
- [33] Zhu W, Bian X, Xie Q. Refined seismic fragility curves of substation equipment considering ground motion classifications. Soil Dyn Earthq Eng 2024;187 (September):108995. https://doi.org/10.1016/j.soildyn.2024.108995.
- [34] Jalayer F. Direct probabilistic seismic analysis: implementing nonlinear dynamic assessment. Stanford University; 2003.
- [35] Institute of Electrical and Electronics Engineers IEEE. Recommended practices for seismic design of substations IEEE 693, 2018; 2018.
- [36] CIGRÉ, "Recomendación de requisitos sísmicos para instalaciones eléctricas de alta tensión," Santiago, Chile, 2020. [Online]. Available: https://www.cigre.cl/p ublicaciones/REQUISITOS-SISMICOS-PARA-INSTALACIONES-ELECTRICAS-AT.
- [37] CNE, "Norma técnica de seguridad y calidad de servicio," Santiago, Chile, 2019. [Online]. Available: https://www.cne.cl/wp-content/uploads/2020/01 /NTSyCS-Dic2019.pdf.
- [38] CNE, "Anexo técnico: exigencias mínimas de diseño de instalaciones de transmisión," Santiago, 2018. [Online]. Available: https://www.cne.cl/wp-content/uploads/2020/09/EXIGENCIAS-MÍNIMAS-DE-DISEÑO-DE-INSTALACIONES-DE-TRANSMISIÓN.pdf.
- [39] Dueñas-Osorio L, Vemuru SM. Cascading failures in complex infrastructure systems. Struct Saf 2008;31(2):157–67. https://doi.org/10.1016/j. strusafe.2008.06.007.
- [40] Alvarez V, Hernández R, Novacovic I. Información técnica del sistema eléctrico nacional nomenclatura de instalaciones. Coord Elétrico Nac 2021 [Online]. Available: https://infotecnica.coordinador.cl/documents/58/Nomenclat ura_de_Instalaciones_V6.0.pdf.
- [41] I. of E. and E. E. IEEE. Graphic symbols for electrical and electronics diagrams, 315. IEEE; 1975.
- [42] CEN, "Sistema eléctrico nacional." https://www.coordinador.cl/sistema-electrico/ (accessed Dec. 21, 2022).
- [43] CEN. Infotécnica. 2022. https://infotecnica.coordinador.cl/ (accessed Dec. 21, 2022)
- [44] Hwang HHM, Huo JR. Seismic fragility analysis of electric substation equipment and structures. Probab Eng Mech 1998;13(2):107–16. https://doi.org/10.1016/ s0266-8920(97)00017-9.
- [45] Song J, Der Kiureghian A, Sackman JL. Seismic response and reliability of electrical equipment and systems. PEER Rep 2005;2005-16.
- [46] CSI, "SAP2000 integrated software for structural analysis and design." Computers and Structures Inc., Berkeley, California.
- [47] Castro S, Benavente R, Crempien JG, Candia G, de la Llera JC. A consistently processed strong-motion database for Chilean earthquakes. Seismol Res Lett 2022; 93(5):2700–18. https://doi.org/10.1785/0220200336.
- [48] Baker JW, Lee C. An improved algorithm for selecting ground motions to match a conditional spectrum. J Earthq Eng 2018;22(4):708–23. https://doi.org/10.1080/ 13632469.2016.1264334.

- [49] MINVU, "Diseño Sísmico de Edificios," D. Of. No. 40133, Decreto Supremo N 61, 2011.
- [50] Zhao JX, et al. Attenuation relations of strong ground motion in Japan using site classification based on predominant period. Bull Seismol Soc Am 2006;96(3): 898–913. https://doi.org/10.1785/0120050122.
- [51] Montalva GA, Bastías N, Rodriguez-Marek A. Ground-motion prediction equation for the Chilean subduction zone. Bull Seismol Soc Am 2017;107(2):901–11. https://doi.org/10.1785/0120160221.
- [52] Kuehn NM, Bozorgnia Y, Campbell KW, Gregor N. A regionalized partially nonergodic ground-motion model for subduction earthquakes using the NGA-Sub database. Earthq Spectra 2023;39(3):1625–57. https://doi.org/10.1177/ 87552930231180906
- [53] Parker GA, Stewart JP, Boore DM, Atkinson GM, Hassani B. NGA-subduction global ground motion models with regional adjustment factors. Earthq Spectra 2022;38 (1):456–93. https://doi.org/10.1177/87552930211034889.
- [54] Abrahamson NA, Gulerce Z. Summary of the Abrahamson and Gulerce NGA-SUB ground-motion model for subduction earthquakes. Earthq Spectra 2022;38(4): 2638–81
- [55] Strasser FO, Arango MC, Bommer JJ. Scaling of the source dimensions of interface and intraslab subduction-zone earthquakes with moment magnitude. Seism Res Lett 2010;81(6):941–50. https://doi.org/10.1785/gssrl.81.6.941.
- [56] Poulos A, Monsalve M, Zamora N, de la Llera JC. An updated recurrence model for chilean subduction seismicity and statistical validation of its poisson nature. Bull Seismol Soc Am 2019;109(1):66–74. https://doi.org/10.1785/0120170160.
- [57] Baker JW. Efficient analytical fragility function fitting using dynamic structural analysis. Earthq Spectra 2015;31(1):579–99. https://doi.org/10.1193/ 021113F0S025M
- [58] Cimellaro GP, Roh H, Fahad M, Reinhorn AM, Schiff A. Modeling combined friction-viscous damping in response of hollow core composite insulators. Struct Congr 2010;2010:2736–47. https://doi.org/10.1061/41130(369)247.
- [59] Roh H, Oliveto ND, Reinhorn AM. Experimental test and modeling of hollow-core composite insulators. Nonlinear Dyn 2012;69(4):1651–63. https://doi.org/ 10.1007/s11071-012-0376-4.
- [60] Barlow RE, Proschan F. Statistical theory of reliability and life testing: probability models. Holt, Rinehart, and Winston; 1975.
- [61] Navarro J. Introduction to system reliability theory. Springer; 2022. https://doi. org/10.1007/978-3-030-86953-3. eBook ISBN: 978-3-030-86953-3.
- [62] Yun S, Jung J. Analyzing temporary overvoltage by the non-islanding operation of distributed generation in multi-grounded neutral distribution system. Int J Electr Power Energy Syst 2022;137(September 2021):107822. https://doi.org/10.1016/ i.iignes.2021.107822.
- [63] Cerretti A, Gatta FM, Geri A, Lauria S, MacCioni M, Valtorta G. Ground fault temporary overvoltages in MV networks: evaluation and experimental tests. IEEE Trans Power Deliv 2012;27(3):1592–600. https://doi.org/10.1109/ TPWRD.2012.2192456.
- [64] Muñoz Gálvez JP, D'Ayala D, Palazzi NC, de la Llera JC. A new procedure to derive typological fragility functions for unreinforced masonry structures: an application to a Chilean case. Bull Earthquake Eng 2025;23:4119–57. https://doi.org/ 10.1007/s10518-025-02190-1.